Multiphased tectonic evolution of the Central Algerian margin from combined wide-angle and reflection seismic data off Tipaza, Algeria

A. Leprêtre,[1] F. Klingelhoefer,[2] D. Graindorge,[1] P. Schnurle,[2] M. O. Beslier,[3] K. Yelles,[4] J. Déverchère,[1] and R. Bracene[5]

Received 23 October 2012; revised 4 July 2013; accepted 30 July 2013; published 26 August 2013.

[1] The origin of the Algerian margin remains one of the key questions still discussed in the Western Mediterranean sea, due to the imprecise nature and kinematics of the associated basin during the Neogene. For the first time, the deep structure of the Maghrebian margin was explored during the SPIRAL seismic survey. In this work, we present a N-S transect off Tipaza (west of Algiers), a place where the margin broadens due to a topographic high (Khayr-al-Din Bank). New deep penetration seismic profiles allow us to image the sedimentary sequence in the Algerian basin and the crustal structure at the continent-ocean boundary. Modeling of the wide-angle data shows thinning of the basement, from more than 15 km in the continental upper margin to only 5–6 km of oceanic-type basement in the Algerian basin, and reveals a very narrow or absent transitional zone. Analysis of the deep structure of the margin indicates features inherited from its complex evolution: (1) an oceanic-type crust in the deep basin, (2) similarities with margins formed in a transform-type setting, (3) a progressive deepening of the whole sedimentary cover, and the thickening of the Plio-Quaternary sediments at the margin foot, coeval with (4) a downward flexure of the basement in the basin. These features argue for a multiphased evolution of the margin, including (1) an early stage of rifting and/or spreading, (2) a late transcurrent episode related to the westward migration of the Alboran domain, and (3) a diffuse Plio-Quaternary compressional reactivation of the margin.

Citation: Leprêtre, A., F. Klingelhoefer, D. Graindorge, P. Schnurle, M. O. Beslier, K. Yelles, J. Déverchère, and R. Bracene (2013), Multiphased tectonic evolution of the Central Algerian margin from combined wide-angle and reflection seismic data off Tipaza, Algeria, *J. Geophys. Res. Solid Earth*, *118*, 3899–3916, doi:10.1002/jgrb.50318.

1. Introduction

[2] Research on continental passive margins is largely focused on the understanding of rifting processes and mechanisms of lithosphere thinning leading to continental breakup and spreading. The way in which continental margins exhibit various structural styles according to the setting of rifting, inheritance, magmatic supply, and/or mantle conditions during their formation is well studied [e.g., *Bown and White*, 1994; *Louden and Chian*, 1999; *Geoffroy*, 2005; *Ziegler and Cloetingh*, 2004]. Nevertheless, during rifting and/or subsequent oceanic spreading stages, the above factors, together with the geodynamical setting, may evolve, conferring to the margins a complex structure. In addition, rifting in back-arc basins might be different in some points from cratonic rifting, though the mechanics of actual fracturing of the continental crust remains similar. The main difference between back-arc and cratonic rifting is the presence of a subducting slab in the mantle beneath the back-arc basin [*Currie and Hyndman*, 2006; *Dunn and Martinez*, 2011].

[3] The North African Algerian passive continental margin results from back-arc opening of the Western Mediterranean basin during Oligo-Miocene times [*Schettino and Turco*, 2006]. While the opening histories of the neighboring basins (Liguro-Provençal and Tyrrhenian basins, Figure 1) are fairly well understood today [*Gueguen et al.*, 1998; *Jolivet and Faccenna*, 2000; *Rosenbaum et al.*, 2002], the mechanisms for the opening of the Algerian basin are still controversial regarding (1) the rifting processes (asymmetric, symmetric), (2) the rate and direction of opening, and (3) the postrift evolution of its southern margin. This is

[1] Domaines océaniques, UMR 6538, Institut Universitaire Européen de la Mer, Université de Bretagne Occidentale, Plouzané, France.
[2] Department of Marine Geosciences, Ifremer, Plouzané, France.
[3] Université de Nice Sophia-Antipolis, CNRS (UMR 7329), Observatoire de la Côte d Azur, Valbonne, France.
[4] Centre de Recherche en Astronomie Astrophysique et Géophysique, Algiers, Algeria.
[5] SONATRACH Exploration, Boumerdès, Algeria.

Corresponding author: A. Leprêtre, Domaines océaniques, UMR 6538, Institut Universitaire Européen de la Mer, Université de Bretagne Occidentale, place Nicolas Copernic, 29280 Plouzané, France. (angelique.lepretre@univ-brest.fr)

2169-9313/13/10.1002/jgrb.50318

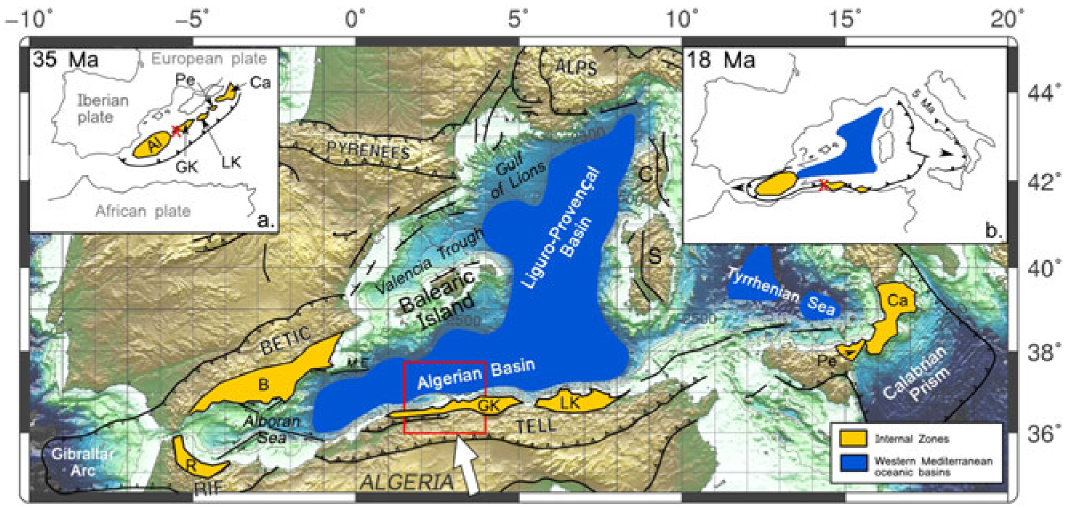

Figure 1. Present-day tectonic map of the Western Mediterranean area. Bathymetry and topography are from ETOPO1 1 min Global relief (*www.ngdc.noaa.gov*). Major tectonics feature are from *Frizon de Lamotte et al.* [2000] and *Billi et al.* [2011]. The white arrow shows velocity of the African plate relative to the stable European plate (~5 mm/yr) from GPS measurements [*Nocquet and Calais*, 2004]. The red rectangle marks the location of the region displayed in Figure 2. The two insets show the Western Mediterranean setting (a) at 35 Ma and (b) at 18 Ma, simplified and modified from *Lonergan and White* [1997], with the migration of the Internal Zones behind the Tethyan subduction front and the associated back-arc opening of the Algerian basin. The red cross shows the approximative position of our study area. C: Corsica, S: Sardinia, GK: Great Kabylia, LK: Lesser Kabylia, Pe: Pelorian, Ca: Calabria, Al: Alboran, B: Betic, R: Rif., M.E: Mazarron Escarpment.

especially due to the lack of knowledge on the deep geometry of the basin and surrounding margins. The Algerian margin is now one of the few examples of a margin that experienced a tectonic inversion, resulting in the recent and actual compressional field [*Serpelloni et al.*, 2007] attested by the seismicity as well as tectonic and kinematic evidences [*Yelles et al.*, 2009].

[4] Because of its setting, the Central Algerian margin (Tipaza region, west of Algiers) is a key area for attempting the reconstruction of tectonic evolution in this southern part of the Western Mediterranean sea and for understanding the modification of passive margins by reactivation processes. Furthermore, it is the only place where a large-scale tilted block, called the Khayr-al-Din Bank and inherited from the rifting stage, is proposed to be present [*El Robrini*, 1986; *Domzig et al.*, 2006; *Yelles et al.*, 2009; *Strzerzynski et al.*, 2010].

[5] Among the major unsolved questions, we would like to address the following points: (1) What is the nature and thickness of the crust underlying the Algerian basin? (2) Where is the ocean-continent transition, and what is its origin? (3) What is the nature and deep geometry of the Khayr-al-Din Bank? (4) Is there evidence for deep markers of margin reactivation? (5) What are the implications of these results on models for the evolution of the Algerian basin and its southern margin?

[6] In order to unravel the deep geometry and structures of the Maghrebian margin both onshore and offshore, the SPIRAL (Sismique Profonde et Investigations Régionales en Algérie) project was launched in September 2009 in collaboration between Algerian scientific institutions (Sonatrach; Centre de Recherche en Astronomie, Astrophysique et Geophysique; and Directorate-General for Scientific Research and Technological Development) and French Research organizations (Centre National de la Recherche Scientifique, Institut Français de Recherche pour l'Exploitation de la Mer (Ifremer), Institut de Recherche pour le Développement, and universities). Specifically, new wide-angle seismic transects, together with coincident multichannel seismic (MCS) data provide the first constraints on the margin's deep structure, on the nature of the ocean-continent transition (OCT), and the associated Algerian basin, as well as on the recent compressive reactivation at crustal scale. In this study we present first results from a deep seismic transect across the Central Algerian margin based on forward modeling of wide-angle seismic data and a coincident multichannel seismic profile and compare it with other margins of the Western Mediterranean sea and the Atlantic ocean.

2. Geological Setting

2.1. The Algerian Margin

[7] The Algerian margin corresponds to the plate boundary between the European and African plates. It is bounded to the north by the Algerian basin and to the south by an Alpine-type belt called Maghrebides (known as the "Tell" north Algeria, Figure 1), resulting from the subduction and closure of the Tethyan ocean under the European plate in Miocene times [*Auzende et al.*, 1973; *Frizon de Lamotte et al.*, 2000].

[8] The evolution of the Algerian margin is closely related to the rollback of the Tethyan slab and the related back-arc opening of the Western Mediterranean basins (Figure 1).

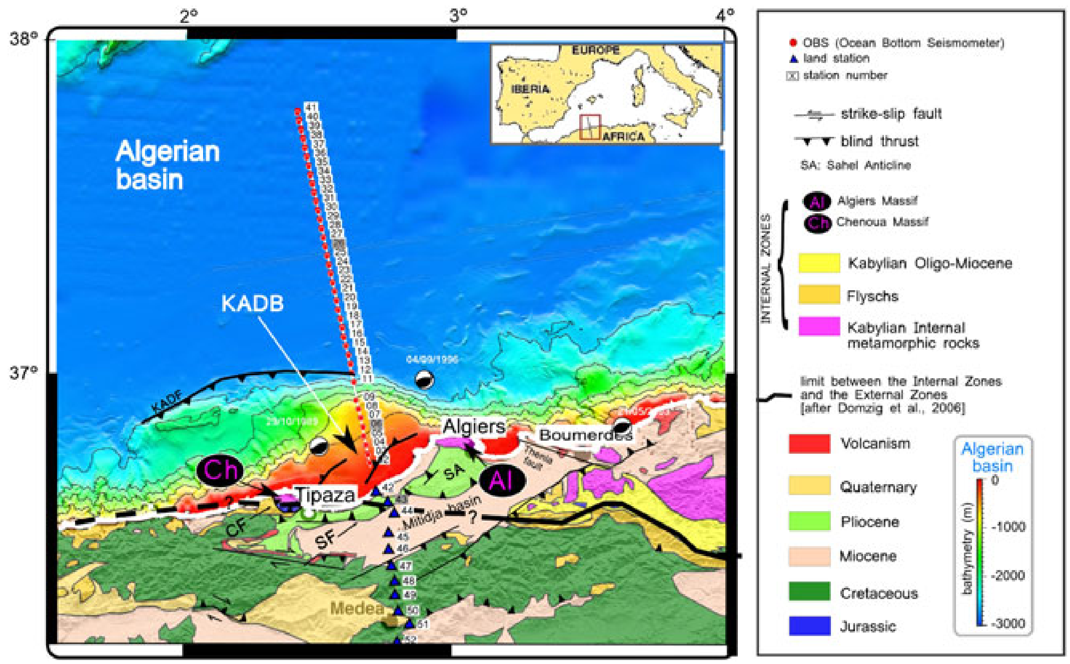

Figure 2. Location of the wide-angle seismic profile in the Bou Ismail Bay, sector of Tipaza. Ocean bottom seismometer (OBS) positions are marked by red circles and the land stations by blue triangles. The numbers of the stations shown in Figure 6 are shaded. The multichannel seismic profile Spi06 is indicated with a white line. The geological and tectonic framework on land is extracted from *Yelles et al.* [2009]. KADF: Khayr-al-Din fault, CF: Chenoua fault, SF: Sahel fault, SA: Sahel anticline, Al: Algiers massif, Ch: Chenoua massif.

There is a general consensus that the Algero-Provençal basin opened during late Oligocene-early Miocene times in a back-arc position behind the Tethyan subduction zone [*Jolivet and Faccenna*, 2000; *Gelabert et al.*, 2002; *Speranza et al.*, 2002]. In the early Miocene, the stretching of the European plate is assumed to have caused the drifting, spreading, and finally the collision of parts of a continental block, the Internal Zones, called AlKaPeCa (for Alboran, Kabylies, Peloritan, and Calabria; *Bouillin* [1986]), with the African continent (Figure 1a). Currently, those Internal blocks are scattered around the Western Mediterranean basin, part of them having been accreted along the Algerian margin, such as the Kabylian blocks (Figure 1).

[9] Models of the opening of the Algerian basin remain controversial regarding the kinematics and nature of the margins: (1) Some authors promote an opening of this basin at the rear of a double subduction toward the west (Alboran) and the east (Calabria) [*Malinverno and Ryan*, 1986; *Lonergan and White*, 1997], after the Kabylian collision with the African plate (18 Ma), resulting in a dominant E-W opening between 16 and 8 Ma behind the Gibraltar arc roll-back and Alboran block migration toward the west [*Mauffret et al.*, 2004]. The westward migration of the Alboran block [*Mauffret et al.*, 2004] would have induced a left-lateral deformation along the Western and Central Algerian margins and right-lateral deformation along the Balearic Promontory [*Camerlenghi et al.*, 2009] (Figure 1b). (2) Other authors propose an older NW-SE opening of the Algerian basin behind the retreating of a subduction zone toward the S-SE, whereas no significant displacement (i.e., less than ~200 km) of the Alboran block is considered [*Gueguen et al.*, 1998; *Gelabert et al.*, 2002; *Lonergan and White*, 1997 and *Schettino and Turco*, 2006]. Whatever model chosen, the westernmost Algerian margin can be assumed to represent a purely strike-slip type margin [*Domzig et al.*, 2006], having formed as a STEP-fault system (subduction-transform edge propagator, *Govers and Wortel* [2005]).

[10] The Algerian margin and basin are then marked by a major salinity crisis during Messinian times, which affected the whole Western Mediterranean domain and surrounding margins (~5.96–5.32 Ma, *Hsu et al.* [1973]; *Gautier et al.* [1994]; *Krijgsman et al.* [1999]). This event resulted in the progressive closure of the connection between the Atlantic Ocean and the Mediterranean Sea, responsible for a total sea level fall of more than 1500 m [*Ryan and Cita*, 1978]. It led to an intense erosion of the basin margins, the accumulation of erosional products in the downslope domain [*Savoye and Piper*, 1991; *Sage et al.*, 2005], and the deposition of the thick evaporitic Messinian sequences in the deep Mediterranean basin [*Montadert et al.*, 1970; *Hsu et al.*, 1973; *Lofi et al.*, 2011] responsible for marked salt tectonics. The Messinian units form a good temporal seismic marker, easily recognizable in the Mediterranean area.

[11] The Plio-Quaternary period was then characterized by the tectonic inversion of the Algerian margin. This major tectonic episode is still in progress and contributes to the general structure of the Algerian margin. Recent kinematic studies indicate a present-day shortening associated with the NW-SE [*Stich et al.*, 2006] convergence between the African and European plates of about 5–6 mm/yr at the longitude of Algiers [*Nocquet and Calais*, 2004] (Figure 1). A significant part (between 1.6 and 2.7 mm/yr) of the deformation may

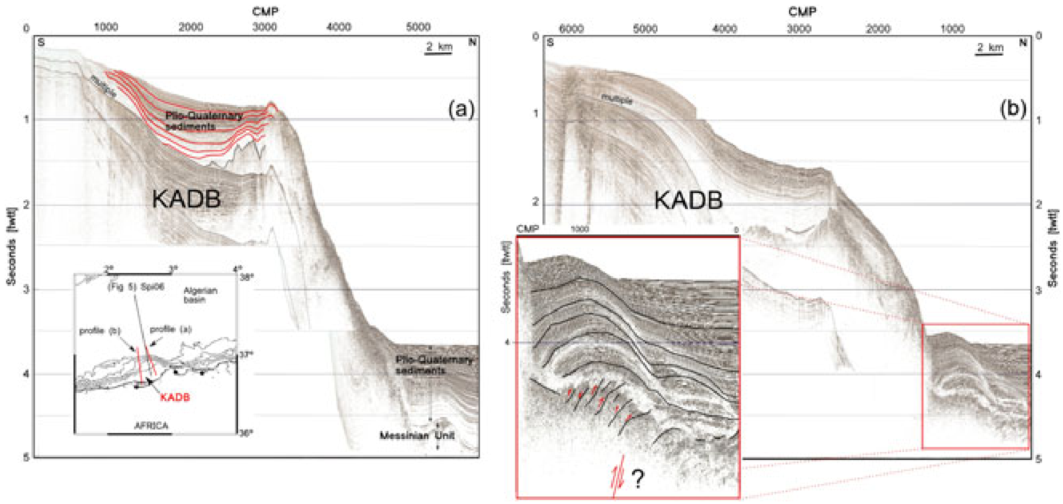

Figure 3. High-resolution seismic profiles from the MARADJA cruise (2003) across the Khayr-al-Din Bank (modified after *Yelles et al.* [2009] (vertical exaggeration: 9). The position of each line is indicated by red lines on the map, and the deep seismic profile SPIRAL Spi06 is indicated by the black line. (a) Seismic section showing the steep northern slope of the banc toward the deep basin, and the sedimentary sequence at the top of the banc and at its foot. (b) Seismic section across the central part of the banc. The inset shows the compressive bulge at the foot of the margin identified by *Yelles et al.* [2009], which is assumed to be related to the presence of a south dipping blind thrust beneath the KADB.

currently occur offshore Algeria (*Serpelloni et al.* [2007]; *Meghraoui et al.* [1996], respectively), and even further north in the SE Iberian margin [*Maillard and Mauffret*, 2013].

[12] Contractional deformation is supported by the existence of dominantly reverse-type fault plane solutions in the present seismicity, as exemplified by earthquakes of Chenoua ($M_w = 6.0$, 1989 [*Bounif et al.*, 2003]), Ain Benian ($M_w = 5.7$, 1996), and Boumerdès ($M_w = 6.8$, 2003 [*Delouis et al.*, 2004]) (Figure 2). In recent papers, authors describe active offshore structures as folds and south dipping blind thrusts both east and west of Algiers [*Domzig et al.*, 2006; *Déverchère et al.*, 2005; *Yelles et al.*, 2009; *Strzerzynski et al.*, 2010], one of them being tentatively related to the destructive Boumerdès earthquake in May 2003 and attesting to the recent compressional reactivation of the margin (Figure 2). The inversion of the Algerian margin remains an active process, and the North African margin could represent an early stage of incipient subduction, as first suggested by *Auzende et al.* [1972] and later by *Yelles et al.* [2009] and *Strzerzynski et al.* [2010], based on recent studies conducted on the Khayr-al-Din Bank, a bathymetric high in the region of Tipaza (Figure 2). This area is thus assumed to have recorded all the tectonic episodes that have affected the Algerian margin, from the rollback of the Tethyan slab to the recent compressional reactivation of the margin.

2.2. Sector of the Khayr-al-Din Bank (KADB)

[13] West of Algiers, the continental shelf significantly widens and forms the bathymetric high of the Khayr-al-Din Bank (KADB, Figure 2). This structure extends over ~80 km in a roughly E-W direction and 45 km in a N-S direction, overlooking the deep basin of about 2000 m depth (Figure 2). The northern KADB limit shows a steep slope with a basinward dip of about 12° (Figure 3a). It is bordered onshore by the Sahel structure, the Chenoua and Algiers Internal massifs to the west and the east, respectively (Ch and Al, Figure 2), and to the north by the deep Algerian basin.

[14] The KADB was recently investigated using morphological and high-resolution seismic data (MARADJA 2003 and 2005 cruises [*Déverchère et al.*, 2005; *Domzig et al.*, 2006, *Yelles et al.*, 2009; *Strzerzynski et al.*, 2010]) and is interpreted as a tilted block inherited from the rifting of the Algero-Provençal basin, as first suggested by *El Robrini* [1986]. It is also assumed to represent relics of the Kabylian basement, originally part of the Internal Zones, and the offshore extension of the Chenoua and Algiers internal massifs which outcrop onshore [*Domzig et al.*, 2006; *Strzerzynski et al.*, 2010] (Figure 2).

[15] Evidence for recent compression is indicated by the presence of an asymmetric ~100 m high bulge at the foot of the slope visible in the morphology and imaged by seismic reflection profiles from the MARADJA cruise (Figure 3b). The asymmetric steeper northern flank of the bulge and the associated basement uplift could be controlled by an active south dipping thrust system located beneath the Khayr-al-Din Bank, although this structure is not directly imaged [*Domzig et al.*, 2006; *Yelles et al.*, 2009] (Figure 3b). In north Algeria, structures inherited from the Miocene phase are generally characterized by a southward vergence, like the Miocene suture bordering the Internal Zones to the south, whereas newly formed reverse structures from the reactivation exhibit an opposite northward vergence [*Yelles et al.*, 2009; *Déverchère et al.*, 2005] (Figure 2).

3. Seismic Data

3.1. Data Acquisition

[16] A wide-angle seismic profile close to Tipaza and the coincident MCS cross-section Spi06 are presented in

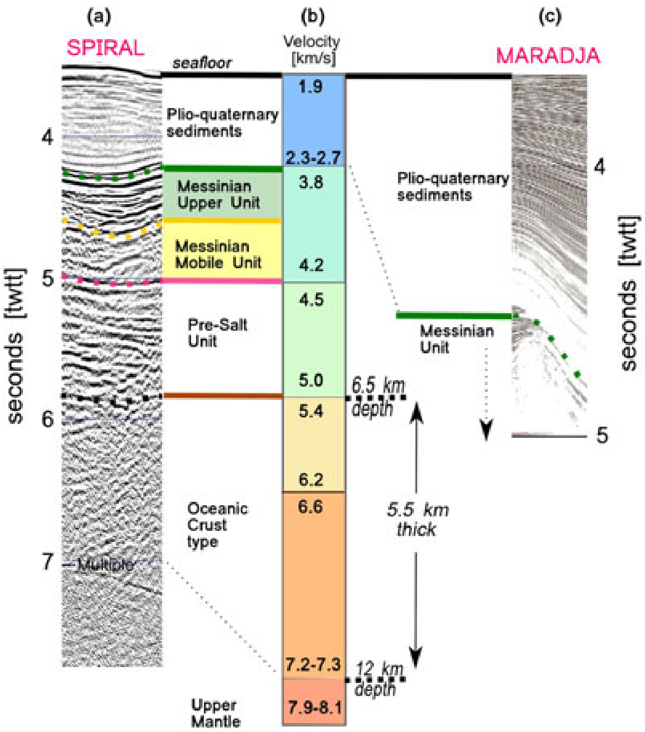

Figure 4. (a) Stratigraphic units identified on the line Spi06 in the deep Algerian basin, (b) their correlations with velocities from the velocity forward modeling (this study), and with (c) high-resolution seismic reflection data from the MARADJA cruise (profile a, Figure 3).

this work (Figure 2). Deep seismic data were acquired during the SPIRAL cruise conducted on the R/V *L'Atalante* (IFREMER) in October–November 2009. Thirty-nine four-component ocean bottom seismometers (OBS) spaced at 3 km interval were deployed along the 120 km NNW-SSE profile across the western Algerian margin (Bou Ismail bay) offshore, and 23 land stations were also deployed, extending the marine transect by 110 km on land. The seismic profile crosses the deep basin, the Khayr-al-Din Bank, the Sahel structure, and the Mitidja basin (Figure 2).

[17] Two different seismic sources were used during the cruise in order to achieve two objectives: (1) The MCS profile Spi06 coincident with the wide-angle line off Tipaza presented in this study was acquired using a seismic airgun array of 13 airguns of various volumes (synchronized on the first bubble) to generate 2299 shots of low frequency (maximum frequency of ~70 Hz) to allow for deep penetration of the seismic signal [*Avedik et al.*, 1993]. This source provided a total volume of 50 L, with an intershot of 20 s leading to 50 m spacing. Our objective was to increase the seismic coverage to allow for better processing results. (2) For the wide-angle acquisition, a seismic airgun array composed of eight airguns of 16 L and two airguns of 9 L was used to generate 751 low-frequency shots, synchronized on the first peak. This source provided a total volume of 146 L, with an intershot of 60 s leading to 150 m spacing. Simultaneously with the wide-angle acquisition, the coincident MCS profile Spi25 was acquired. All MCS profiles were recorded, using the 4.5 km streamer of Ifremer, composed of 360 12.5 m channels. MCS and OBS data were recorded with a sample rate of 4 ms.

3.2. Multichannel Seismic (MCS) Data and Processing

[18] The SPIRAL seismic sources were chosen to image deep targets, such as the top and the base of the crust, the OCT, and the deep rooting of the structures. Therefore, the deep penetrating and low-frequency MCS data set is complementary to the high-resolution and superficial data acquired during the MARADJA cruises (2003 and 2005) and was used to image deep structures underneath the salt layer (Figures 4 and 5). A first quality control was undertaken on groups of traces using the SISPEED software, and further processing of the MCS data was then performed using the GEOCLUSTER software. The processing sequence included external and internal mutes, spherical divergence correction, bandpass filtering (3–5–95–105 Hz), and dynamic corrections. Two consecutive velocity analyses were conducted every 200 CMP (common midpoint) leading to the final stack. The last processing step was the application of a frequency-wavenumber migration on the data using a constant 1550 km/s water velocity. The Spi06 profile exhibits a higher resolution than the Spi25 profile, due to the higher frequencies of the source. Therefore, the MCS interpretation presented in this paper is based on the Spi06 profile, whereas interfaces from MCS data integrated during the forward modeling (see the next section) were picked from the Spi25 profile to avoid even minimal differences in time and/or space between MCS and wide-angle arrival times. The wide-angle seismic data aids geological interpretation of the crust by providing deeper and complementary information such as P-wave velocities (Vp) on the structure of the margin.

3.3. Seismic Velocity Modeling of the Wide-Angle Seismic Data

[19] The refraction data were modeled using forward modeling technique, taking into account first as well as secondary arrivals from OBS and land stations, and reflectors picked from the coincident multichannel seismic section (Figure 7).

3.3.1. Data Quality and Preprocessing of the Wide-Angle Seismic Data

[20] OBS data were corrected for clock-drift, and seafloor positions were calculated using the direct water wave. A preprocessing sequence was applied to all data (land stations and OBS) in order to increase the signal-to-noise ratio and to better image far-offset arrivals. This sequence is composed of a deconvolution whitening, a 3–17 Hz Butterworth filter, and an automatic gain control.

[21] The OBS data acquired along the Tipaza profile are of good quality, with a better signal-to-noise ratio on the vertical geophone component than on the hydrophone. The OBS sections show clear sedimentary (Ps1, Ps2, Ps3) and crustal arrivals (Pg1, Pg2), and deep arrivals from the upper mantle (Pn) are identifiable (Vp $\geq$ 7.6 km/s) up to 50 km offset away from some OBS (Figures 6a and 6b). Sedimentary reflections (PsP1, PsP2) as well as reflections from the top of the basement (PgP) are clearly observed in the deep basin. Moho reflections (PmP) are not always easily discernible in the deep Algerian basin, even after applying the preprocessing sequence. For the forward modeling, picking

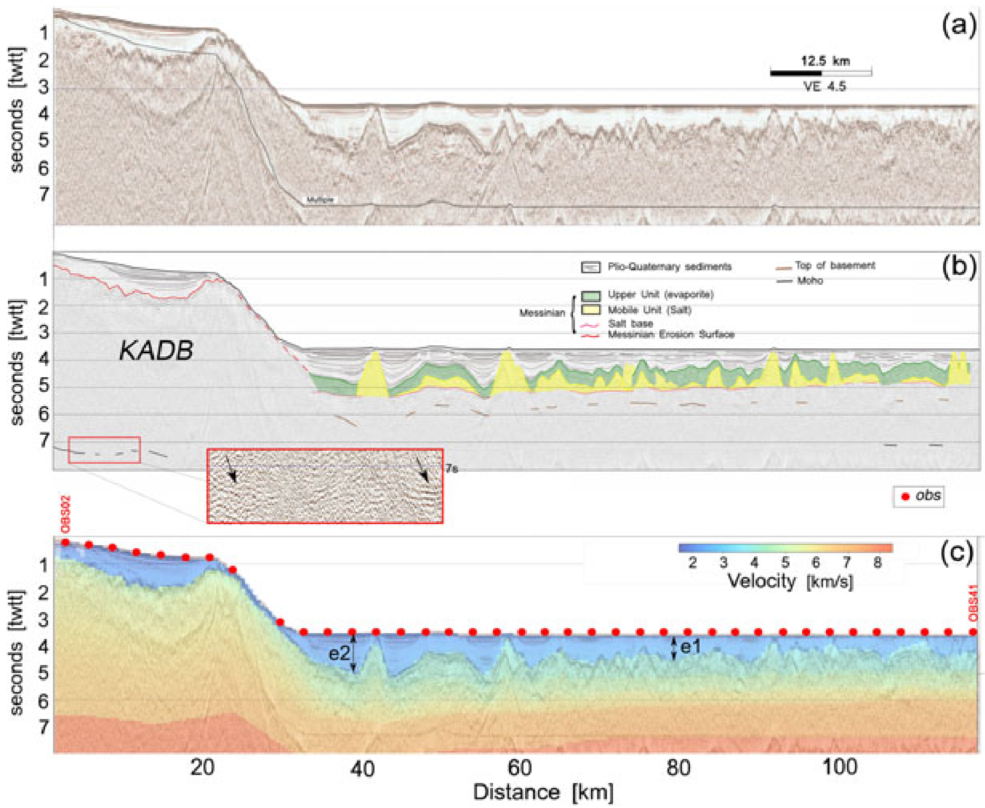

Figure 5. (a) Time migrated multichannel seismic profile Spi06. (b) A corresponding line drawing showing the deepening of both the top and the base of the Messinian units and several deep reflections. The inset shows deep reflection of low amplitude probably corresponding to the Moho discontinuity beneath the KADB at 7.2–7.5 s, and (c) section Spi06 with velocities from forward modeling (Figure 7) converted in time underlain. KADB: Khayr-al-Din Bank. Plio-Quaternary sediment thicknesses presented in section 4.3 are estimated using the forward model in "e1" and "e2" (see details in the text).

uncertainties were defined for each phase using the method of *Zelt* [1999], based on the ratio of the amplitude 250 ms before and after the picked arrival. A mean error depending on the signal-to-noise ratio was calculated from all the picks, for each phase of each station, and then converted to a traveltime picking errors, for a range in values between 20 and 125 ms. Phases with a high ratio are characterized by a low uncertainty, whereas phases with a low ratio are characterized by a higher uncertainty. Phases names and picks are detailed in Table 1. Wide-angle data acquired in the deep basin are rather homogeneous, whereas data recorded close to the coastline show significant lateral variations, probably induced by strong changes in bathymetry and by lateral structural variations, especially in the crustal part of the profile (Figures 6a and 6b).

[22] Among the 23 land stations deployed, only 11 exhibited a sufficient quality to allow picking identification of arrivals. Most of them were located close to the coastline (Figure 7). Land station sections did not show sedimentary arrivals due to the large distance between the station and the closest shot but only deep arrivals (PmP, Pg) (Figure 6c). Pn arrivals from the upper mantle were not recorded by the land stations.

3.3.2. Forward Modeling

[23] Construction of a forward ray tracing model allows us on the one hand to include information from reflected phases and multichannel data into the model and, on the other hand, to verify that all structures from the forward model are required to fit the data. For the modeling, a minimum structure for the continental crust was used to successfully explain arrivals at the land stations.

[24] Seismic velocities were modeled using the 2-D ray tracing software XRAYINVR developed by *Zelt and Smith* [1992]. This modeling used a layer-stripping strategy, from the top of the model downward. The velocity model is constructed layer after layer and composed of velocity and interface nodes. Depth and velocities were modeled such as to minimize the difference between the observed arrival times and the arrival times computed in the model (Figures 6 and 7).

[25] The set of observed traveltimes, including refracted and reflected phases, were picked from the 39 OBS and 11 land stations recorded sections. Geometries of the sedimentary layers were determined from interfaces picked from the MCS coincident line. These interfaces include the Messinian erosion surface on the upper margin, as well as the top of the Messinian units, and, where visible, the base of the Messinian salt layer in the deep basin (see geological units, Figures 4 and 5). Arrival times picked from the MCS data were converted to depth using velocities from the forward modeling. For these layers, only the velocities were adjusted to reduce the misfit between observed

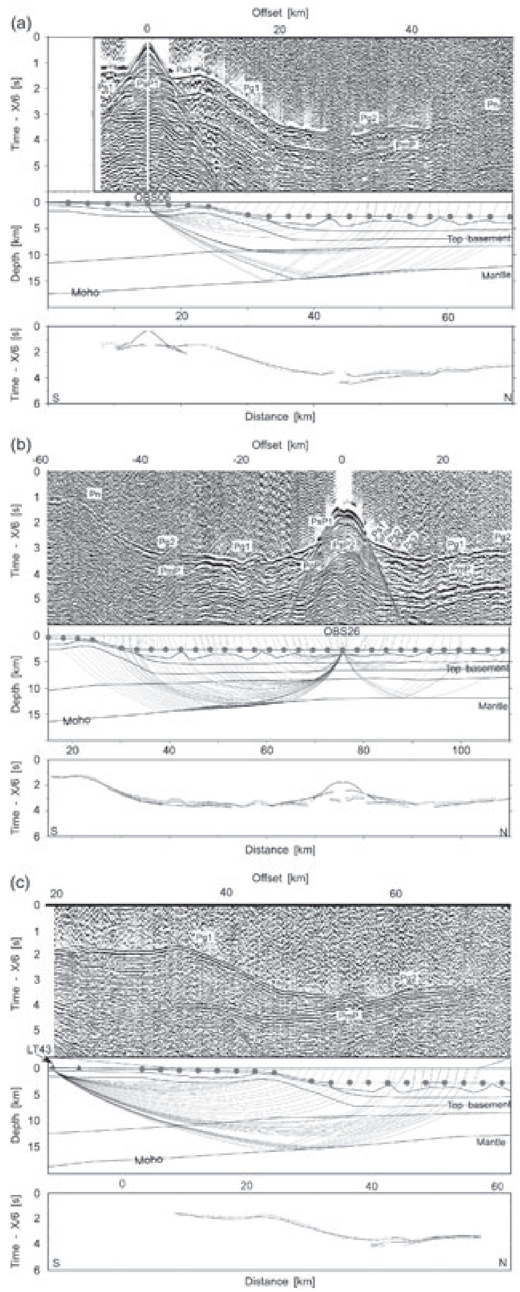

Figure 6. Three examples of representative record sections (wide-angle data). (a) Seismic section of OBS 06 on the upper margin (top), the corresponding ray paths in the forward model (middle), and the observed traveltime picks (thick grey lines) and calculated traveltimes (thin black lines) in the forward model (bottom). (b) Seismic section of OBS 26 in the deep basin (top), the corresponding ray paths in the forward model (middle), and the observed traveltime picks (thick grey lines) and calculated traveltimes (thin black lines) in the forward model (bottom). (c) Seismic section of land station 43 (top), the corresponding ray paths in the forward model (middle), and the observed traveltime picks (thick grey lines) and calculated traveltimes (thin black lines) in the forward model (bottom). These three stations are shaded in Figure 2. All the examples correspond to the vertical component recording, represented with a 6 km/s velocity reduction.

and calculated traveltimes. The forward modeling integrated 28,586 picks.

3.3.3. Error Analyses

[26] The quality of the forward model can be quantified using the fit between predicted arrival times and traveltime picks. The corresponding misfit is 121 ms using 93% of the picks. The number of picks, RMS errors, and χ^2 for each phase obtained for the final forward model are detailed in Table 1.

[27] Two-point ray tracing between source and receiver (Figure 8) shows the well-resolved and the unconstrained areas. Ray coverage for both diving and reflected waves is generally very good due to the excellent data quality and close instrument spacing (Figures 8a and 8b). All sedimentary layers are well sampled by reflected and turning rays in the marine part of the model. The crustal layers, the oceanic Moho, and the upper mantle are well sampled.

[28] Resolution is a measure of the number of rays passing through a region of the model constrained by a particular velocity node and is therefore dependent on the node spacing [*Zelt*, 1999]. If a layer can be modeled with one single velocity gradient, then the resolution parameter will be high even in areas which have lower ray coverage, as the area is related to only one velocity node. Nodes with values greater than 0.5 are considered well resolved (Figure 9). The velocities throughout the model show a resolution higher than 0.5 except at the southern end of the model. The resolution decreases at the ends of the model where no rays pass through the layers and also decreases at the very shallow onshore sedimentary layer due to missing reverse shots on land. Upper mantle velocities are well constrained at higher levels, however less so at increasing depth due to fewer rays penetrating into this deeper portion of the model.

[29] In order to estimate the velocity and depth uncertainty of the final velocity model, a perturbation analysis was performed. The depths of key interfaces were varied, and an *F* test was applied to determine if a significant change between models could be detected. The 95% confidence limit gives an estimate of the depth uncertainty of the interface (Figures 9 and 10). In order to better constrain uncertainty at the Moho, both the depth of this interface and velocities in the lower crustal layer were changed systematically (Figure 10). We obtain on our final model uncertainties of +0.3/–0.4 km and $\pm$0.1 km/s for the Moho depth and for velocities in the lower crust, respectively. Results from this analysis show that our preferred model allows a maximum of picks to be explained, with a minimum resulting misfit between the picked traveltimes and arrivals predicted from the modeling. Solutions leading to better fits explain a lower number of picks and are thus less reliable.

[30] In order to additionally test the validity of the forward velocity model, we may also convert velocity to density using an empirical law. This density model is then used to generate a predicted gravity anomaly which can be compared with the measured gravity anomaly. The gravity anomaly was modeled using the software GRAVMOD [*Zelt and Smith*, 1992] and free-air gravity anomaly data collected during the SPIRAL cruise. This modeling approach is based on the empirical relationship existing between seismic velocities and densities proposed by *Ludwig et al.* [1970]. The misfit between calculated and predicted gravity

Table 1. Residual Traveltimes and Chi-Square Errors for All the Phases for the Tipaza Transect, Using Forward Modeling

Phase	Name	Number of Picks	RMS [s]	χ^2 Error	Uncertainties
Water		1893	0.014	0.460	0.020–0.035
Sediment refraction in the Plio-Quaternary unit	Ps1	748	0.086	1.261	0.020–0.100
Sediment refraction in the Messinian units	Ps2	1695	0.104	0.761	0.100–0.125
Sediment refraction in the Presalt unit	Ps3	1494	0.132	1.895	0.020–0.125
Reflection at the top of the Messinian unit	PsP1	1710	0.072	6.330	0.025–0.050
Reflection at the base of the Messinian Salt unit	PsP2	1263	0.097	2.399	0.100–0.125
Reflection at the top of the basement	PgP	1465	0.128	3.256	0.020–0.125
Refraction in the upper crust	Pg1	4562	0.137	1.232	0.125
Refraction in the lower crust	Pg2	6037	0.121	1.456	0.100–0.125
Reflection at the Moho	PmP	5866	0.142	1.403	0.100–0.125
Refraction in the upper mantle	Pn	1853	0.127	1.073	0.100–0.125
	All Phases	28586	0.121	1.720	

anomalies is about 15.5 mGal, which represents a good validation of our velocity forward model (Figures 7a and 7b). The largest misfit observed, between 15 and 30 km model distance, might be due to the 3-D topography of the KADB (Figure 7).

4. Results

[31] Forward modeling was carried out and coupled with the interpretation of the MCS data on the marine part of the seismic profile in order to (1) constrain the structure of the sedimentary sequence and the basement of the Algerian margin and basin off Tipaza and (2) better understand the kinematic and tectonic history of the Algerian margin. The main sedimentary and crustal features identified are described below.

4.1. Structure of the Sedimentary Units

[32] While the MARADJA data were limited by their penetration (Figures 3 and 4), the MCS profile SPIRAL

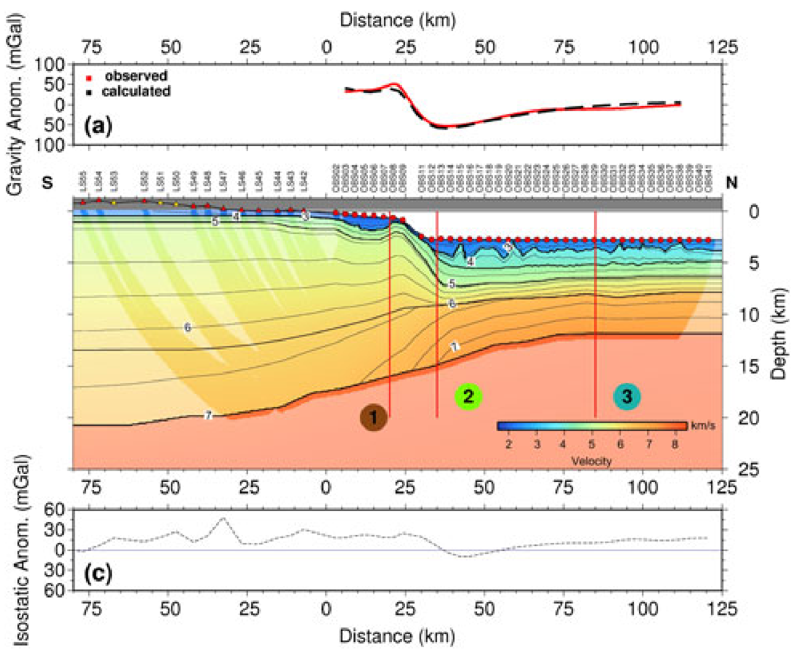

Figure 7. Results of forward velocity and gravity modeling along the Tipaza profile. (a) Results of the gravity modeling. Red line represents gravity anomalies from the SPIRAL cruise measurement, and the dashed black line represents gravity anomalies calculated from conversion of the seismic velocity predicted by the forward modeling to densities. (b) Results of the forward velocity modeling, including 39 OBS and 11 land stations. OBS locations are indicated by red circles. Locations of the land stations used in the modeling are indicated by red triangles. Seismic records from the land stations indicated by yellow triangles are of too low a quality to be integrated. Isovelocity contours are represented every 0.25 km/s. Areas unconstrained by ray tracing are shaded. Red lines mark velocity-depth profiles shown in Figure 11. (c) Isostatic gravity anomaly calculated along the transect assuming a local isostatic equilibrium and constant values of 2700 and 3300 kg/m^3 for crust and mantle densities, respectively [e.g., *Behn and Lin*, 2000; *Balmino et al.*, 2012], and a level of compensation at a depth of 15 km. Density for the crust is chosen to be typical of continental crust. The Bouguer gravity anomaly is from the International Gravimetric Bureau (BGI) (*http://bgi.omp.obs-mip.fr/*) (see text for details).

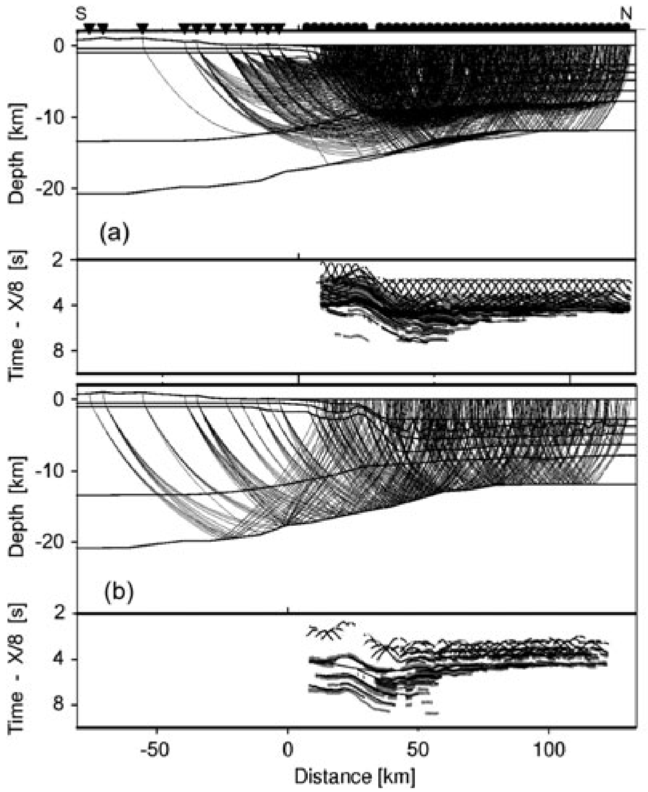

Figure 8. (a) (top) Ray coverage of diving waves with every twentieth ray from two-point ray tracing plotted. (bottom) Observed traveltime picks and calculated traveltimes (line) for the same phases for all receivers along the model. (b) Same as Figure 8a but for reflected phases.

Spi06 (Figure 5) and the coincident wide-angle data define the overall geometry of the margin and locally allow to image below the salt layer and farther toward the deep basin (until about 120 km away from the Algerian coast). From the upper margin toward the deep Algerian basin, we can discern three structural regions:

[33] 1. The top of the KADB is marked by a perched sedimentary basin filled with several kilometers of Plio-Quaternary (~1.2 km thick) and Miocene sediments (~1 km thick). This basin is imaged on the Spi06 profile at the top of the bank (Figure 5), where the Messinian Erosion Surface (MES) forms a depression. It is visible in the forward model by an area of low velocities where isovelocity contour deepens at the top of the bank between distances of 5 and 25 km (Figure 7).

[34] 2. A sharp 12° slope forms the northern border of the KADB which marks the transition from the upper margin to the Algerian basin. On the slope between OBS 8 and OBS 11 (see location, Figures 2 and 7), only a few Ps1 phases were observed, and no PsP and no PgP phases were recorded. Across this second region, the Plio-Quaternary unit is very thin and the slope particularly steep, rendering the modeling difficult.

[35] 3. In the deep basin, evidence for intensive salt tectonics, including local diapirs that outcrop at the seafloor, is imaged by multichannel and wide-angle seismic data (Figures 5 and 6). Tall salt diapirs at the margin foot induce strong undulations of the refracted arrivals on the OBS sections (Figures 6a and 6b).

[36] In the deep basin, variations in sediment thickness are observed at two scales: (i) At short wavelengths, both the Plio-Quaternary sediments (1.9 km/s $\leq$ Vp $\leq$ 2.7 km/s) and the Messinian sequence (3.9 km/s $\leq$ Vp $\leq$ 4.20 km/s) exhibit strong variations in thickness associated with diapirism induced by the Messinian salt. Below these levels, the deepest presalt sedimentary layer (Figure 4) shows a relatively constant thickness of about 1.3–1.4 km along the basin (Figure 7), with velocities ranging from 4.50 km/s at the top to 5.0 km/s at the base. (ii) At larger wavelengths, the total sedimentary cover depicts a regular 3.7 km thickness corresponding to the sedimentary infilling of the distal basin (Figure 7). However, the whole sedimentary cover shows a progressive thickening toward the margin foot, where it reaches more than 4 km in thickness.

4.2. Structure of the Crust and Upper Mantle Velocities

[37] Beneath the upper margin (KADB), the Moho evolves at a depth greater than 15 km below the southern part of the KADB (distance 0 on model, Figure 7) and becomes progressively shallower toward the deep basin. This results in a crustal thickness of about 15 km where the perched sedimentary basin is observed (between 5 and 20 km in the model, Figure 7). In the MCS data section, the Moho probably corresponds to some discontinuous reflections observed at 7.2–7.5 seconds two-way travel time (stwtt) between 0 and 12 km along the profile (Figure 5b), comparable with the time-converted forward velocity model (Figure 5c). Crustal *P* velocities change from 5.2 km/s in the upper part of the crust to 6.3 km/s in the lower part, resulting in a very low vertical velocity gradient of 0.065 $\pm$ 0.015 km/s/km.

[38] The transition toward the deep basin is marked by a thinning of the crust from more than 15 km thick in the upper margin to only ~6 km at the margin foot (Figure 7), over a distance of 50 km. Underneath the sedimentary cover, the basement is characterized by a two-layered velocity structure and depicts an average total thickness of ~5.5 km in the deep Algerian basin (Figure 7). Velocities evolve from 5.4 to 6.2 km/s in the upper layer and from 6.6 to 7.2–7.3 km/s across the lower layer (Figure 4). The crust in this region can be modeled using only one layer, as no strong

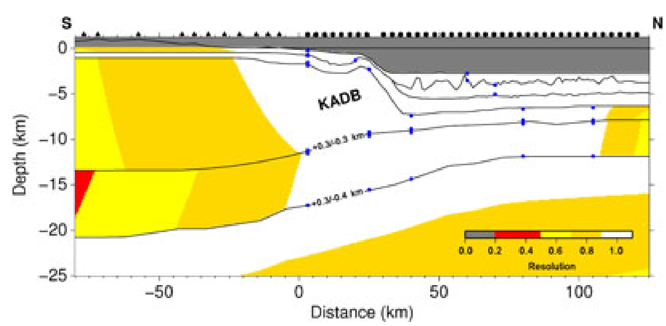

Figure 9. Resolution parameter for depth nodes of the velocity model. The depth uncertainties of the most important boundaries calculated from the 95% confidence limit of the f-test are given in the framed boxes (Figure 10). Velocity nodes are indicated by blue circles.

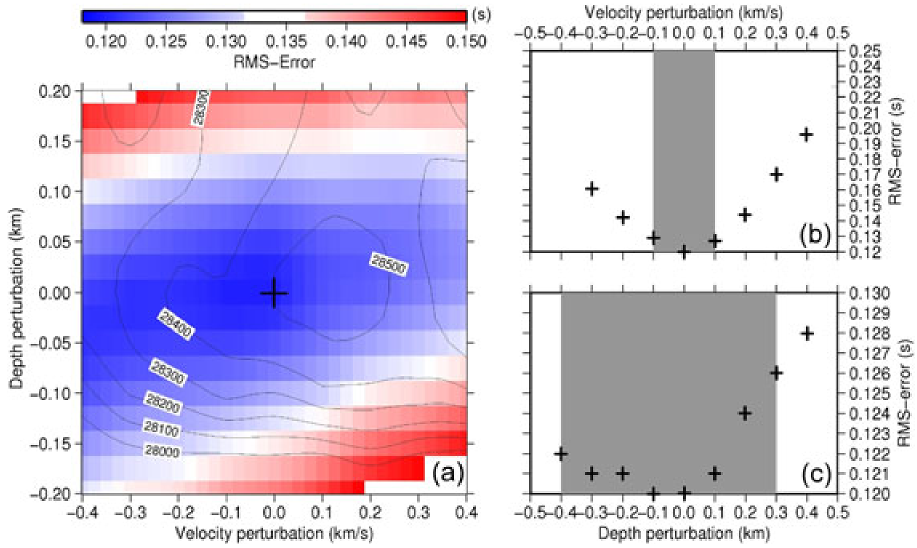

Figure 10. Error analysis by model perturbation. (a) Results from simultaneous variation of the depth of the Moho and velocities in the lower crustal layer. Contours indicate the number of picks explained by the forward model. The uncertainties of the most important boundaries calculated from the 95% confidence limit of the f-test are given in the grey boxes. (b) Results from variation of the lower crustal velocities only. (c) Results from variation of the Moho depth. The uncertainties of the most important boundaries calculated from the 95% confidence limit of the f-test are given in the grey box.

reflections from intracrustal boundary are clear in the data. However, as a first arrival tomographic modeling performed on the marine part clearly images two layers, an upper layer characterized by a high velocity gradient and a lower layer with a weak gradient, we use a two-layered velocity model for this region. There, in the distal deep basin, the top of the crust is located at a constant depth of ~6.5 km (~5.5 stwtt) and the Moho discontinuity at ~12 km (~7 stwtt) (Figures 5 and 7). Both the top and the base of the crust, as well as the isovelocity contours, slightly deepen toward the margin foot where the sedimentary cover is thicker (Figure 7).

[39] The southern end of the model, between –80 and 0 km (Figure 7), corresponds to the onshore part. There, the sedimentary layers cannot be imaged by the seismic data because of the large offset between land stations and offshore shots. Land stations do not provide a good resolution on land but rather help us to constrain the deep structure of the margin with the contribution of Pg and PmP arrivals (Figure 6c). At the southern end of the model, the deep arrivals enable us to model the Moho depth between –35 and 0 km in the profile where it reaches ~20 km depth at about 35 km from the coastline (Figure 7).

[40] Upper mantle velocities are constrained by Pn arrivals between distances of 20 and 115 km along the forward model (Figure 8a). The velocities range from 7.9 to 8.0 km/s just below the crust, when using velocities of 8.2–8.3 km/s at 30 km depth during modeling. PmP arrivals reflected on the Moho beneath the margin foot and the deep basin are of lower amplitude when compared with those reflected beneath the KADB (Figure 6). This observation supports a lower velocity contrast between crustal and mantle velocities at the transition between lower crust and upper mantle along Domains 2 and 3 relative to Domain 1, where velocities are lower at the base of the crust.

4.3. Nature of the Crust

[41] According to 1-D velocity-depth profiles from forward modeling (Figure 11), three different domains can be distinguished along the transect (Figure 7). These profiles were compared with preexisting compilations of velocity-depth profiles extracted from below the top of the basement, for typical thinned continental crust [*Christensen and Mooney*, 1995] and Atlantic-type oceanic crust [*White et al.*, 1992] in order to provide information on the nature of the basement across the different domains.

[42] 1. The first domain corresponds to the upper margin marked by the Khayr-al-Din Bank (Domain 1, Figure 7). It is located between 0 and 30 km from the coastline. In this domain, the crust shows velocities and a velocity gradient consistent with typical continental crust (curve 1, Figure 11). The vertical velocity gradient is low, and the velocities are lower than those of oceanic-type crust. The velocity-depth profile falls into the range of velocities compiled by *Christensen and Mooney* [1995] of velocities for an extended continental crust type (Figure 11). The continental nature and geometry of the KADB support the hypothesis of its origin as a block inherited from the rifting stage, as proposed in earlier work [*El Robrini*, 1986; *Domzig et al.*, 2006; *Yelles et al.*, 2009].

[43] 2. The second domain is located at the foot of the margin, between 30 and 40 km along the section (Domain 2, Figure 7). In this area, the model depicts intermediate velocities faster than in typical continental crust and slower than in typical oceanic crust (Figure 11), in a very narrow transition zone (~10 km wide or less). However, the resolution of our velocity model does not allow us to discriminate between a narrow transition zone or direct contact between continental and oceanic crust.

[44] 3. The third domain is located beneath the deep basin at ~ 40 km from the coastline, toward the north

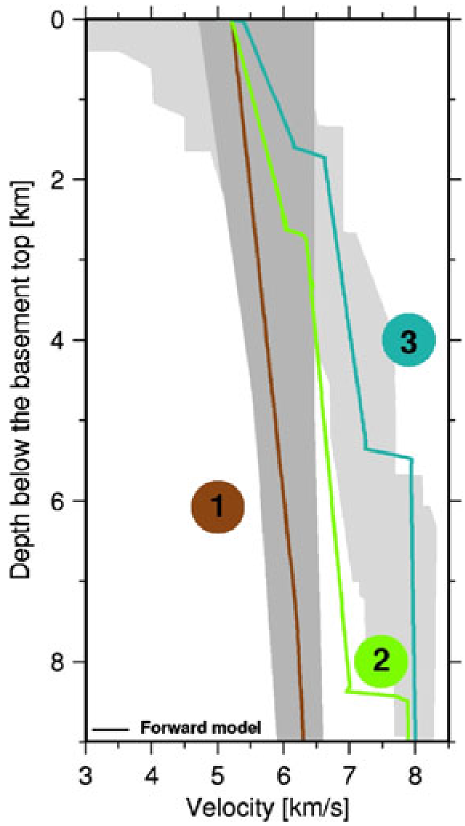

Figure 11. The 1-D velocity/depth profiles in the basement extracted from forward velocity model at distances of 20 (curve 1), 35 (curve 2), and 85 km (curve 3) along the model. The dark grey area represents a velocity compilation for extended continental crust extracted from *Christensen and Mooney* [1995], and the light grey area represents a velocity compilation for Atlantic oceanic crust from *White et al.* [1992].

(Domain 3, Figure 7). Here velocities are too high to correspond to an extended continental crust but are consistent with an oceanic-type crust (curve 3, Figure 11). The 1-D velocity-depth profile reveals a two-layer structure for the basement, with a high velocity gradient in the upper part (0.7±0.1 km/s/km) and a lower gradient in the lower part (0.3±0.06 km/s/km), typical of the so-called *layer 2* and *layer 3* in oceanic crust [*White et al.*, 1992]. Its total thickness is relatively constant at approximately 5.5 km, which is less than the thickness of an Atlantic-type oceanic crust (~7 km), whereas velocities in the lower crust (*layer 3*) reach up to 7.2–7.3 km/s and thus are at the upper bound of velocities of typical Atlantic oceanic crust [*White et al.*, 1992]. These velocities at the base of the *layer 3* are continuous between Domains 2 and 3.

4.4. Sedimentary and Crustal Geometry at the Margin Foot

[45] Four main observations can be made about the sedimentary and crustal geometry: (1) In the deep basin, the whole sedimentary cover thickens at the margin foot. Only Plio-Quaternary sediments show a significant variation in thickness in the deep basin, toward the margin foot. The thickness of the Plio-Quaternary layer changes from an average of 0.9 km (e1, Figure 5) in the deep basin between diapirs, to 1.6 km (e2, Figure 5) at the margin foot, indicating a thickening of about 700 m. (2) Along our section, the top of the Messinian sediments as well as the base of the Messinian salt progressively deepen toward the continent. The top of the Messinian sequence evolves from 4.1 to 4.75 stwtt (Figure 5), equivalent on the forward model to a depth of 3.6 to 4.5 km (Figure 7), whereas the base of the Messinian salt evolves from about 4.8 stwtt at the northern end of the Spi06 profile to 5.3 stwtt at the margin foot, equivalent in the forward model to a depth of 4.9 km in the northern part to a depth of 5.5 km at the margin foot (Figures 5 and 7). (3) The thickening of the Plio-Quaternary sequence and the long-wavelength deepening of the top of the Messinian layer toward the continent (Figure 5) are coincident with a south dipping trend in the basement top (Figure 7). (4) The steep slope of the northern border of the KADB may be another indication for compressional reactivation of the Algerian margin in the study area associated with a verticalization of the block, as suggested by *Yelles et al.* [2009].

5. Discussion

5.1. Deep Structure of the Algerian Margin and Its Basin (Sector of Tipaza)

[46] Our velocity modeling together with the MCS data provides us an image of the sedimentary and crustal structure of the Algerian basin and of the ocean-continent transition zone. The deep structure of the margin is discussed here in its upper, lower, and transitional parts defined in the previous section, which can be distinguished from their seismic structure and the nature of the basement.

5.1.1. Continental Crust (Domain 1)

[47] At the upper margin formed by the KADB, the velocity structure as well as the crustal thickness are typical of thinned continental crust [*Christensen and Mooney*, 1995] (Figure 11), with indications for the existence of a possible former tilted block. Both the continental nature and the location of the KADB between the two Algiers and Chenoua Internal massifs outcropping onshore (Figure 2) favor an origin of the KADB basement from the Internal Zones. The northern boundary of the bank would thus represent the sharp offshore border of these European paleo-terranes, off Tipaza. Beyond the bank, the smooth topography and the velocity structure of the basement exclude any tilted blocks farther north. South of the bank, the location of the southernmost Internal Zones boundary is difficult to define due to the lack of geological outcrops and the presence of the Neogene Mitidja basin (Figure 2). Nevertheless, it might be found close to the coastline because of the presence of the External domain (paleo-African margin [*Bouillin*, 1986]) farther south.

[48] On land, between the coast and southward along the profile (Figure 7b), the Moho deepens and reaches ~20 km depth at about 50 km from the coastline. This shallow Moho depth on land compared with the topography seems to involve a local undercompensation of the area. In order to test this hypothesis, the Bouguer gravity anomaly from the BGI was used to estimate the gravity isostatic anomaly [*Balmino et al.*, 2012, and references therein] for the land part. We modeled the Bouguer gravity anomaly expected in

the case of a local isostatic compensation of the topography (Airy-type, i.e., elastic thickness $Te = 0$). By subtracting this anomaly from the Bouguer gravity anomaly of the BGI, we obtained an estimate of the way the relief is compensated below the margin on land (Figure 7c). The positive anomaly observed on land suggests that the area is characterized by a mass excess relative to an Airy-type compensation. If we assume that the mass excess is linked to the crust-mantle density contrast, then the Moho is shallower than expected in an Airy-type model, suggesting an undercompensation of the margin on land. This result is thus in good agreement with our finding of a relatively shallow Moho at the coastline (Figure 7b).

[49] This isostatic disequilibrium could be related to a major thermal event linked to a suspected break-off of the Tethyan slab (~16–17 Ma ago [see, e.g., *Maury et al.*, 2000]), which is assumed to have effected the mantle beneath the north Algerian domain. Two main factors may explain this relatively shallow position of the Moho on land between the coast and southward along the profile (Figure 7): (1) A "rollback factor" which might explain the thinned continental crust observed along the southern margins of the Western Mediterranean Sea, where parts of Internal Zones are accreted to previously active-type margins (West Sardinian margin [*Gailler et al.*, 2009]; West Calabrian margin [*Pepe et al.*, 2010]). Those specific areas are made of crustal material from the Internal Zones and thus have been affected by back-arc extension during the rollback of the Tethyan slab which would have induced crustal thinning at depth. (2) Inheritance from the old African passive margin, which previously represented a thinned domain before collision of the Internal Zones, might also contribute to the shallow position of the Moho on land along our profile [e.g., *Roure et al.*, 2012].

5.1.2. Oceanic Crust in the Deep Basin (Domain 3)

[50] Wide-angle seismic studies reveal variations in thickness of the oceanic crust globally. Generally, proximity of hotspots, abnormally hot asthenosphere conditions, and/or a fast spreading environment might result in unusually thick oceanic crust, whereas abnormally thin oceanic crust is found at slow to ultraslow-spreading centers, in proximity to fracture zones, and/or in the case of cold mantle conditions [e.g., *White et al.*, 1992; *Bown and White*, 1994]. The thickness of the oceanic crust is thus the result of complex tectonic and magmatic processes operating during accretion.

[51] The oceanic crust (Domain 3) in the Western Mediterranean basin off Africa is thinner (5.5 km [*Hinz*, 1973; *Vidal et al.*, 1998; *Grevemeyer et al.*, 2011; this study]) than "classical" slow-spreading Atlantic oceanic crust type (~7 km thick) but appears comparable to those found in back-arc basins (Liguro-Provençal basin [*Pascal et al.*, 1993; *Contrucci et al.*, 2001; *Gailler et al.*, 2009]; Lau basin [*Turner et al.*, 1999; *Crawford et al.*, 2003]; Philippine sea and Parece Vela basin [*Louden*, 1980]; Japan sea [*Hirata et al.*, 1992]), provided that the crustal thickness is taken away from the influence of any spreading center and/or magmatic arc. The seismic structure of the crust and velocities of 7.2–7.3 km/s at the base of *layer 3* favor an oceanic crustal nature (Figure 11). Wide-angle seismic studies conducted on the South Balearic margin and crossing the north Algerian basin proposed an oceanic crust characterized by velocities ranging from 6.0 km/s at its top and up to 7.4 km/s at its base [*Hinz*, 1973], whereas other authors proposed a thin oceanic crust including velocities lower than 7 km/s (up to 6.8 km/s [*Grevemeyer et al.*, 2011]). These differences may partly result from the different data sets and inversion methods, as well as from geological variations resulting from possible structural segmentation.

[52] Regarding the nature of the crust in the Algerian deep basin off Tipaza, the results of velocity modeling favor an oceanic nature of the basin. The velocity structure together with observed seismic velocities up to 7.2–7.3 km/s were used to exclude a basement of a continental nature in the basin off Tipaza, contrary to the suggestion locally proposed for the Algerian basin by *Roure et al.* [2012].

5.1.3. Ocean-Continent Transition (Domain 2)

[53] The transition between continental and oceanic crust often appears as progressive through a zone neither strictly continental nor oceanic, called the ocean-continent transition (OCT). North of Domain 1 where the continental crust shows a strong thinning toward the deep Algerian basin, the transition between continental and oceanic crust is extremely narrow (10 km or less, Domain 2) and characterized by velocities that are intermediate between continental and oceanic crust (Figure 11) and slightly higher than normal 7 km/s velocities at its base (Figure 7).

[54] For other margins, two main interpretations are proposed for such slightly high velocities at the continent-ocean boundary: (1) volcanic underplating [*Reid and Keen*, 1990; *Bauer et al.*, 2000; *Funck et al.*, 2012] or (2) exhumed continental mantle serpentinized by contact with sea water [*Boillot et al.*, 1989; *Whitmarsh et al.*, 2001; *Funck et al.*, 2004].

[55] Volcanic underplating is typical at volcanic margins where a thick oceanic crust is generally observed [*Bauer et al.*, 2000; *Geoffroy*, 2005] and associated with hot mantle temperature conditions and/or active mantle upwelling [*Holbrook et al.*, 2001; *Korenaga et al.*, 2002]. The reduced thickness of the oceanic crust in the Algerian basin as well as velocities less than 7.3 km/s do not support hypothesis 1, i.e., magmatic underplating and a volcanic-type margin. In addition, magmatic underplating is assumed to generate a double reflection at the top and at the base of the underplating body [*Klingelhoefer et al.*, 2005], as well as seaward dipping reflectors (SRD) at the margin, neither of which are imaged in our data set.

[56] On the other hand, exhumed and serpentinized upper mantle material is often found at continental margins formed with limited or no magmatic activity at the time of continental breakup. Upper mantle serpentinized rock velocities would be compatible with observed velocities higher than 7 km/s found from this study, since seismic velocities are assumed to decrease from normal mantle velocities ($\geq$ 7.9–8.0 km/s) with the increasing degree of serpentinization [*Horen et al.*, 1996]. Nevertheless, PmP reflections are not supposed to be generated at the base of the serpentinized upper mantle, as serpentinization is assumed to occur progressively, without jump in composition and thus in velocity. The specific context of the Algerian margin together with the very low amplitude of the PmP reflections in our data can contradict the purely serpentinized mantle hypothesis 2, even if a serpentinization front is assumed to have generated reflectors observed at the Iberian margin [*Dean et al.*, 2000].

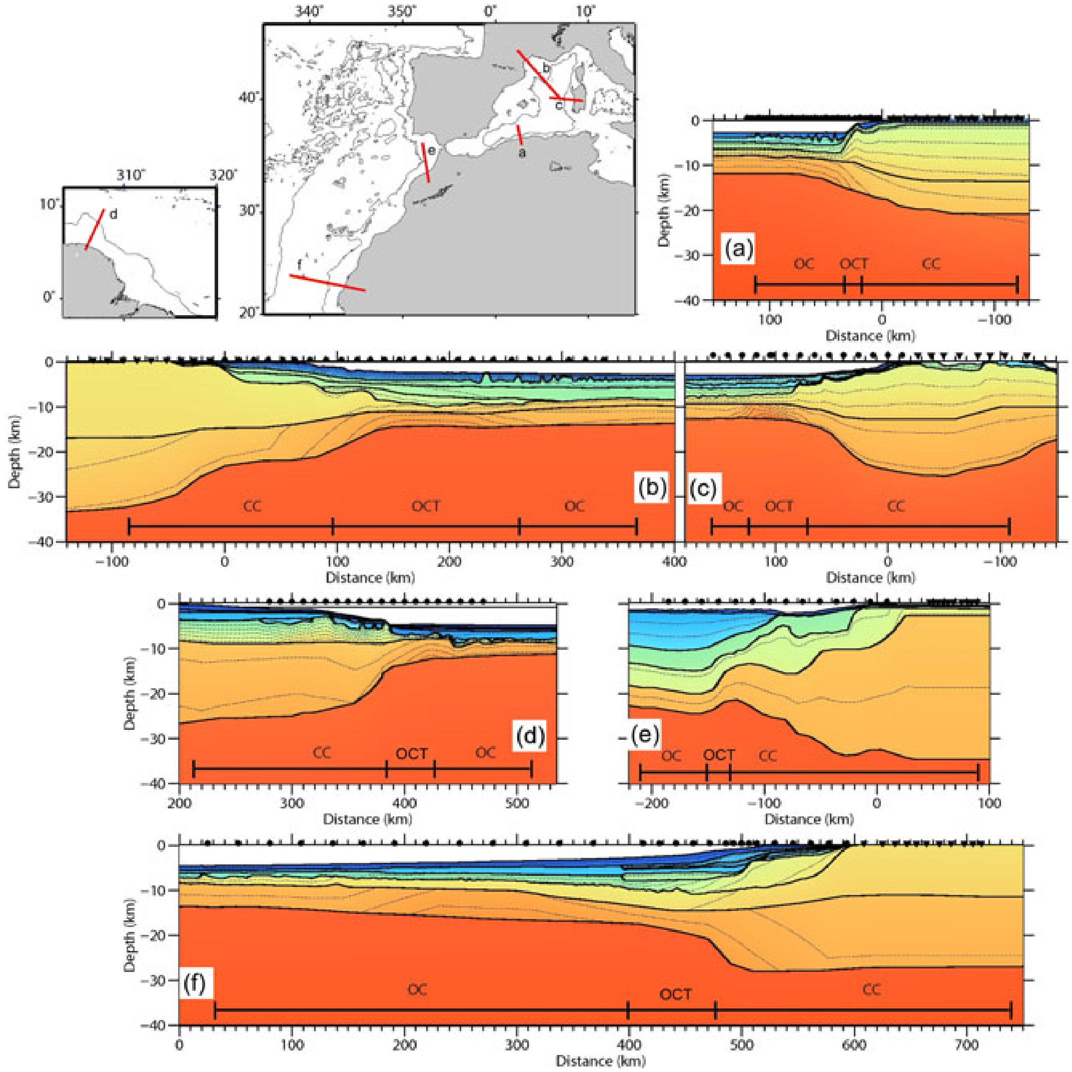

Figure 12. Comparison of the deep structure of three Western Mediterranean margins (lines a, b, and c) and three West Atlantic margins (lines d, e, and f). The locations of the five transects are indicated by a red line on the map. (a) the Algerian margin (this study), (b and c) the conjugate Gulf of Lions-West Sardinia margins [*Klingelhoefer et al.*, 2008; *Gailler et al.*, 2009], (d) the oblique-shear margin of French Guiana [*Greenroyd et al.*, 2008], (e) a transform west Moroccan margin [*Thiébot*, 2005], and (f) the north DAKHLA profile across the west Moroccan margin [*Klingelhoefer et al.*, 2009]. CC: Continental Crust; OC: Oceanic Crust; OCT: Ocean-Continent Transition.

[57] The fast lateral change of velocities in our model, from the continental domain toward the oceanic domain and without major difference with the oceanic velocity structure, favors a very narrow (10 km) or even absent OCT at the Algerian margin off Tipaza.

5.2. Comparison With Other Continental Margins

[58] Until now, no unequivocal interpretation of magmatic anomalies, rifting mechanisms (symmetric, asymmetric), direction, or rate of opening has been proposed for the Algerian basin and surrounding margins [*Schettino and Turco*, 2006; *Mauffret et al.*, 2007, and references therein], leaving open the debate on the type of margin (oblique, transform, or purely divergent) found in this region. Results from this study are compared with the structure and geometry of other passive margins, especially in the Western Mediterranean Sea, to better understand rifting and postrift evolution of the Algerian margin.

[59] The Algerian margin off Tipaza is characterized by a narrow ocean-continent transitional zone compared to other margins of the Western Mediterranean formed in a similar back-arc context. For example, the OCT extends over ~80–90 km in the Gulf of Lions [*Gailler et al.*, 2009] (Figure 12b), ~30–40 km along the North Ligurian and West Sardinian margins [*Rollet et al.*, 2002; *Gailler et al.*, 2009; *Dessa et al.*, 2011] (Figure 12b), and ~20 km at the West Corsican margin [*Contrucci et al.*, 2001; *Rollet et al.*, 2002]. The Gulf of Lions and the West Sardinian Miocene margins represent two conjugate margins, formed during the back-arc opening of the Liguro-Provençal basin in the Western Mediterranean domain (Figure 1). They present a conspicuous asymmetry regarding the dimensions of the

ocean-continent transitional zone (Figure 12), which can be interpreted as the result of a continental breakup closer to the Western Sardinian margin rather than an asymmetry linked to simple shear mechanisms during rifting [*Gailler et al.*, 2009]. That seems to be in agreement with the observation of *Martinez et al.* [2007] that in a back-arc setting, continental breakup occurs preferentially closer to the magmatic arc, which can thus induce asymmetry of the OCT between conjugate margins. For margins formed in a back-arc position, the transition zone at the passive margin born on the same side of the subduction zone with respect to the extended area seems thus to be narrower than the transition zones formed on the opposite side, which can partially explain the narrow OCT found in this study at the Algerian margin. However, the location of the conjugate margin is not well established, a fact which precludes any direct comparison.

[60] A narrow transitional zone is a common feature of margins formed by transcurrent mechanisms (Ghana margin [*Edwards et al.*, 1997; *Sage et al.*, 2000]; NW Moroccan margin [*Thiébot*, 2005]; French Guiana margin [*Greenroyd et al.*, 2008]) (Figures 12d and 12e), which generally depict a direct contact between oceanic and continental crusts for purely transform cases. We thus explore this second hypothesis of transcurrent mechanisms operating during the evolution of Central Algerian margin because of morphological similarities, reminiscent of the geometry observed at Atlantic margins formed in a "shearing" setting [e.g., *Keen et al.*, 1990; *Edwards et al.*, 1997; *Mascle and Basile*, 1998; *Sage et al.*, 2000; *Basile and Allemand*, 2002; *Greenroyd et al.*, 2008; *Basile et al.*, 2013], including (1) a narrow or nonexistent OCT, (2) a steep continental slope toward the deep basin, (3) a marginal basement high, and (4) a reduced region of crustal thinning (Figures 7 and 12). Nevertheless, a steep slope of the Moho toward the continent is usually observed at transform margin [e.g., *Edwards et al.*, 1997] (Figure 12e), contrasting with the gentle slope followed by the Moho beneath the KADB (Figure 12a): this geometry would result from a first stage of rifting before a shearing deformation during the Central Algerian margin evolution.

[61] This hypothesis would imply that the transcurrent mechanisms proposed to have generated the westernmost Algerian margin [*Govers and Wortel*, 2005] could also have effected the margin in the region of Tipaza. Indeed, a recent study has proposed a tectonic reconstruction of the Western Mediterranean at 16 Ma [see *Mauffret et al.*, 2007, Figure 4] that places our study area at the junction between the NW-SE thrust front of the retreating Tethyan slab and the westward migration point of the Alboran block (Figure 1b). North of the Algerian basin, the steep Mazarron escarpment located off Tipaza (Figures 1 and 13c) is often seen as resulting from the westward migration of the Alboran block following the retreating slab [e.g., *Acosta et al.*, 2001; *Camerlenghi et al.*, 2009, and references therein]. Interpreted seismic sections across this escarpment seem to depict structural similarities with a steep slope and perched basin, as imaged by the SPIRAL seismic line across the KADB. These observations may be the expression of transcurrent movements induced by the westward migration of the Gibraltar arc on both sides of the Algerian basin, with a right-lateral motion on the Balearic margin [*Camerlenghi et al.*, 2009] and a left-lateral one on the Algerian margin. Therefore, a possible explanation of the steepness of the margin and the very narrow OCT in our study area could be a multiphased formation of the Algerian margin west of Algiers. This would imply a mixed scenario combining the following:

[62] 1. A roughly N-S rifting at the origin of the remaining thin and tilted continental block (KADB) and opening of the Algerian basin behind the southward rollback of the Tethyan subduction, which explains the nature of the basin and evolution of the Algerian margin farther east [*Lonergan and White*, 1997; *Frizon de Lamotte et al.*, 2000; *Gelabert et al.*, 2002; *Rosenbaum et al.*, 2002].

[63] 2. A later, E-W episode inducing simple shears of opposite directions on both sides of the Algerian basin as a consequence of the Miocene westward migration of the Gibraltar Arc [*Mauffret et al.*, 2007; *Camerlenghi et al.*, 2009].

[64] The comparison shown in Figure 12 highlights common features between the three Western Mediterranean margin examples. The top of the basement of the Mediterranean margins is located in a shallower position relative to those of the Atlantic ocean (Figure 12). This is due to the major subsidence effecting the older Atlantic margins characterized by a denser oceanic basement and a thicker sedimentary cover. Considering the overall structure of the different margins, it appears that the Western Sardinian margin and the Algerian margin present structural similarities. This might result from similarities in their formation. These two margins were (1) formed in a back-arc context, (2) located in an identical position relative to the Tethyan subduction zone, and (3) linked to the migration of the Internal Zones.

5.3. New Evidence for Tectonic Reactivation?

[65] Postbreakup compressional structures are commonly observed at passive or oblique-type continental margins [*Johnson et al.*, 2008]. They are often expressed as fault-related growth folds which appear to result from various driving mechanisms and to strongly depend on (i) preexisting structures, which control the location and the style of reactivation, and (ii) the rheological properties of the lithosphere, which play a key role in the spatial wavelength of compressional deformation [e.g., *Doré et al.*, 2008; *Ritchie et al.*, 2008; *Cloetingh et al.*, 2008].

[66] Numerous data attest to recent and present-day compression in the Algerian offshore, e.g., recent kinematics [*Serpelloni et al.*, 2007], intense seismicity associated with dominant reverse focal mechanisms [*Stich et al.*, 2006], and south dipping blind thrusting [*Déverchère et al.*, 2005; *Domzig et al.*, 2006; *Yelles et al.*, 2009] (Figures 1 and 3). The deep seismic profile Spi06 off Tipaza does not allow us to image directly a south dipping thrust in this location. This may reflect the early stage of compressional deformation which likely has little impact on the geometry of the system to date, provided the slow convergence rate between African and European plates [e.g., *Billi et al.*, 2011, and references therein].

[67] However, it appears that the progressive deepening over several tens of kilometers toward the margin foot of the Plio-Quaternary layer (Figure 5), together with the tilting of the crust beneath the margin, might result from (1) a compressional reactivation of the margin or, alternatively, (2) a crustal flexure associated with a progressive increase in sediment loading. When comparing the Algerian mar-

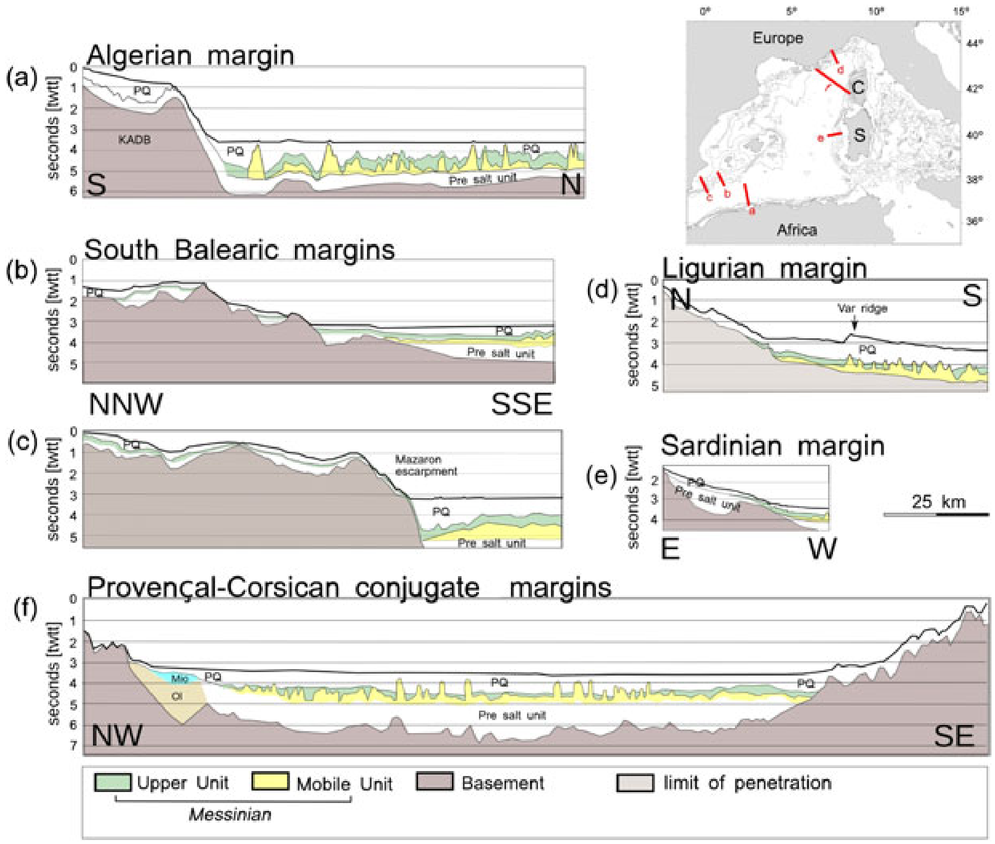

Figure 13. Comparison of five western Mediterranean margins. Profiles across the different margins are represented using the same scale and are marked on the map by red lines. (a) the Algerian margin (this study), (b and c) the south Balearic margin [*Maillard and Mauffret*, 2013], (d) the Ligurian margin [*Lofi et al.*, 2011], (e) the Sardinian margin [*Sage et al.*, 2005], and (f) the Provençal-Corsican conjugate margins [*Rollet et al.*, 2002]. Mio: Miocene sediments; Ol: Oligocene sediments; C: Corsica; S: Sardinia.

gin with other Western Mediterranean margins (Figure 13), i.e., Neogene margins formed in the same general context, a similar sedimentary pattern cannot be observed. Indeed, at long wavelengths, the sedimentary units progressively become shallower from the deep basin toward the continent for the other Mediterranean margins, contrary to what is observed on the Algerian side (Figure 13), even if the sediment load is more or less similar, or even lower in this case. In addition, the shallower position (by at least 1 km) found for the top of a basement and the Moho by *Grevemeyer et al.*, 2011 reveals the deepening of the basement itself from the Balearic Promontory toward the Algerian margin.

[68] Therefore, this peculiar pattern is clearly an additional observation supporting the south dipping underthrusting of the transitional and oceanic crust off north Algeria. This could be the indication of the onset of a subduction process, as previously suggested by *Auzende et al.* [1972], *Domzig et al.* [2006], *Yelles et al.* [2009], *Strzerzynski et al.* [2010], and *Billi et al.* [2011]. There is evidence for a similar phenomenon along the North Iberian margin (South of the Bay of Biscay) during Eocene-Miocene times that has been interpreted as being associated with the Eocene convergence between the European and Iberian plates [*Sibuet*, 1974; *Alvarez-Marron et al.*, 1997; *Gallastegui et al.*, 2002].

6. Conclusions

[69] New wide-angle and reflection seismic data off Tipaza provide a first image of the deep structure of the Algerian margin and the nearby deep basin. Modeling of the wide-angle seismic data reveals an oceanic-type basement of 5–6 km in the deep Algerian basin. The Khayr-al-Din Bank exhibits a continental nature and is likely a tilted block belonging the to the Internal Zones, as supported by geometry found in the velocity model. Between continental and oceanic crusts, there is a very narrow or possibly absent transitional zone (10 km or less). Comparison of the margin structure with that observed in other studies suggests some similarities of the Algerian margin off Tipaza with transform-type margins. Diffuse deformation related to the recent compressional reactivation of the margin is expressed by a long-wavelength flexure of the basin basement and by partial uplift and folding at the KADB. The steep slope of the margin, the progressive deepening of the sedimentary units toward the margins foot coeval with the deepening of

the basement top, and the extremely narrow transition zone between continental and oceanic crusts reveal an atypical margin. This can be explained by a multiphased evolution of the margin including the following majors steps: (1) rollback of the Tethyan subduction zone, inducing (a) the opening of the Central Algerian basin in a roughly N-S to NW-SE direction and (b) the collision of the European inner zone with the African margin, (2) a transcurrent episode induced by the westward migration of the Alboran block, and (3) a compressional reactivation of the margin. The exact timing and modality of these steps remain open questions.

[70] **Acknowledgments.** The authors would like to thank the captain and the crew of the R/V *L'Atalante* of both legs for their professional work during the oceanographic expedition. We would also like to thank the technical team of the Ifremer-UBO OBS pool and the Genavir technical team for their professional work during the deployment of ocean bottom instruments and the acquisition of reflection seismic data. The GMT [*Wessel and Smith*, 1995] and Seismic Unix software package [*Stockwell*, 1999] were used in the preparation of this paper. The authors would like to thank Christopher Greenroyd and Christine Peirce for the use of their ACE wide-angle seismic model and Carole Petit for her help with the isostatic anomaly modeling. Comments of two reviewers helped greatly increase the quality of the manuscript.

References

Acosta, J., A. Munoz, P. Herranz, C. Palomo, M. Ballesteros, M. Vaquero, and E. Uchupi (2001), Geodynamics of the Emile Baudot Escarpment and the Balearic promontory, Western Mediterranean, *Mar. Pet. Geol.*, *18*(3), 349–369, doi:10.1016/S0264-8172(01)00003-4.

Alvarez-Marron, J., E. Rubio, and M. Torne (1997), Subduction related structures in the North Iberian margin, *J. Geophys. Res.*, *102*(B10), 22,497–22,511, doi:10.1029/97JB01425.

Auzende, J. M., J. Bonnin, and J. L. Olivet (1972), Compressive structure of Northern Algeria, *Deep Sea Res.*, *19*(2), 149–155.

Auzende, J. M., J. Bonnin, and J. L. Olivet (1973), The origin of the Western Mediterranean basin, *J. Geol. Soc. London*, *129*, 607–620.

Avedik, F., V. Renard, J. Allenou, and B. Morvan (1993), "Single bubble" airgun array for deep exploration, *Geophysics*, *58*, 366–382.

Balmino, G., N. Vales, S. Bonvalot, and A. Briais (2012), Spherical harmonic modelling to ultra-high degree of Bouguer and isostatic anomalies, *J. Geod.*, *86*(7), 499–520, doi:10.1007/s00190-011-0533-4.

Basile, C., and P. Allemand (2002), Erosion and flexural uplift along transform faults, *Geophys. J. Int.*, *151*(2), 646–653.

Basile, C., A. Maillard, M. Patriat, V. Gaullier, L. Loncke, W. Roest, M. Mercier de Lépinay, and F. Pattier (2013), Structure and evolution of the Demerara plateau, offshore French Guiana: Rifting, tectonic inversion and post-rift at transform-divergent margins intersection, *Tectonophysics*, *591*, 16–29, doi:10.1016/j.tecto.2012.01.010.

Bauer, K., S. Neben, B. Schreckenberger, R. Emmermann, K. Hinz, N. Fechner, K. Gohl, A. Schulze, R. B. Trumbull, and K. Weber (2000), Deep structure of the Namibia continental margin as derived from integrated geophysical studies, *J. Geophys. Res.*, *105*(B11), 25,829–25,853, doi:10.1029/2000JB900227.

Behn, G. D, and J. Lin (2000), Segmentation in gravity and magnetic anomalies along the US East Coast passive margin: Implications for incipient structure of the oceanic lithosphere, *J. Geophys. Res.*, *105*(B11), 25,769–25,790.

Billi, A., C. Faccenna, O. Bellier, L. Minelli, G. Neri, C. Piromallo, D. Presti, D. Scrocca, and E. Serpelloni (2011), Recent tectonic reorganization of the Nubia-Eurasia convergent boundary heading for the closure of the Western Mediterranean, *Bull. Soc. Geol. Fr.*, *182*(4), 279–303.

Boillot, G., G. Feraud, M. Recq, and J. Girardeau (1989), Undercrusting by serpentinite beneath rifted margins, *Nature*, *341*(6242), 523–525.

Bouillin, J. P. (1986), Le bassin maghrébin: Une ancienne limite entre l'Europe et l'Afrique á l'ouest des Alpes, *Bull. Soc. Geol. Fr.*, *8*(4), 547–558.

Bounif, A., M. Bezzeghoud, L. Dorbath, D. Legrand, A. Deschamps, L. Rivera, and H. Benhallou (2003), Seismic source study of the 1989, October 29, Chenoua (Algeria) earthquake from aftershocks, broad-band and strong ground motion records, *Ann. Geophys.*, *46*(4), 625–646.

Bown, J. M., and R. S. White (1994), Variation with spreading rate of oceanic crustal thickness and geochemistry, *Earth Planet. Sci. Lett.*, *121*(3-4), 435–449.

Camerlenghi, A., D. Accettella, S. Costa, G. Lastras, J. Acosta, M. Canals, and N. Wardell (2009), Morphogenesis of the SW Balearic continental slope and adjacent abyssal plain, Western Mediterranean sea, *Int. J. Earth Sci.*, *98*(4), 735–750.

Christensen, N. I., and W. D. Mooney (1995), Seismic velocity structure and composition of the continental-crust—A global view, *J. Geophys. Res.*, *100*(B6), 9761–9788.

Cloetingh, S., F. Beekman, P. A. Ziegler, J. D. Van Wees, and D. Sokoutis (2008), Post-rift compressional reactivation potential of passive margins and extensional basins, in *Nature and Origin of Compression in Passive Margins,* vol. 306, edited by H. Johnson et al., pp. 27–70, Geol. Soc. London Sp. Pub, London.

Contrucci, I., A. Nercessian, N. Bethoux, A. Mauffret, and G. Pascal (2001), A Ligurian (Western Mediterranean Sea) geophysical transect revisited, *Geophys. J. Int.*, *146*(1), 74–97.

Crawford, W. C., D. A Wiens, L. M. Dorman, and S. C. Webb (2003), Tonga Ridge and Lau Basin crustal structure from seismic refraction data, *J. Geophys. Res.*, *108*(B4), 2195, doi:10.1029/2001jb001435.

Currie, C. A., and R. D. Hyndman (2006), The thermal structure of subduction zone back arcs, *J. Geophys. Res.*, *111*, B08404, doi:10.1029/2005JB004024.

Dean, S. M., T. A. Minshull, R. B. Whitmarsh, and K. E. Louden (2000), Deep structure of the ocean-continent transition in the southern Iberia Abyssal Plain from seismic refraction profiles: The IAM-9 transect at 40°20′N, *J. Geophys. Res.*, *105*(B3), 5859–5885.

Delouis, B., M. Vallée, M. Meghraoui, E. Calais, S. Maouche, K. Lamalli, A. Mahsas, P. Briole, F. Benhamouda, and K. Yelles (2004), Slip distribution of the 2003 Boumerdes-Zemmouri earthquake, Algeria, from teleseismic, GPS, and coastal uplift data, *Geophys. Res. Lett.*, *31*, L18607, doi:10.1029/2004GL020687.

Dessa, J. X., et al. (2011), The GROSMARIN experiment: Three dimensional crustal structure of the north Ligurian margin from refraction tomography and preliminary analysis of microseismic measurements, *Bull. Soc. Geol. Fr.*, *182*(4), 305–321.

Déverchère, J., et al. (2005), Active thrust faulting offshore Boumerdes, Algeria, and its relations to the 2003 M_w 6.9 earthquake, *Geophys. Res. Lett.*, *32*, L04311, doi:10.1029/2004GL021646.

Domzig, A., et al. (2006), Searching for the Africa-Eurasia miocene boundary offshore Western Algeria (MARADJA'03 cruise), *C. R. Geosci.*, *338*(1-2), 80–91.

Doré, A. G., E. R. Lundin, N. J. Kusznir, and C. Pascal (2008), Potential mechanisms for the genesis of Cenozoic domal structures on the NE Atlantic margin: Pros, cons and some new ideas, in *Nature and Origin of Compression in Passive Margins,* vol. 306, edited by H. Johnson et al., pp. 1–26, Geol. Soc. London Sp. Pub, London.

Dunn, R. A., and F. Martinez (2011), Contrasting crustal production and rapid mantle transitions beneath back-arc ridges, *Nature*, *469*(7329), 198–202, doi:10.1038/nature09690.

Edwards, R. A., R. B. Whitmarsh, and R. A. Scrutton (1997), Synthesis of the crustal structure of the transform continental margin off Ghana, northern Gulf of Guinea, *Geo-Mar. Lett.*, *17*(1), 12–20.

El Robrini, M. (1986), Evolution morphostructurale de la marge Algérienne occidentale (Méditerranée Occidentale): Influence de la néotectonique et de la sédimentation, PhD thesis, University of Paris IV, p. 164.

Frizon de Lamotte, D., B. A. Saint Bezar, R. Bracene, and E. Mercier (2000), The two main steps of the atlas building and geodynamics of the Western Mediterranean, *Tectonics*, *19*(4), 740–761.

Funck, T., H. R. Jackson, K. E. Louden, S. A. Dehler, and Y. Wu (2004), Crustal structure of the Northern Nova SOCTia rifted continental margin (Eastern Canada), *J. Geophys. Res.*, *109*, B09102, doi:10.1029/2004JB003008.

Funck, T., K. Gohl, V. Damm, and I. Heyde (2012), Tectonic evolution of southern Baffin Bay and Davis Strait: Results from a seismic refraction transect between Canada and Greenland, *J. Geophys. Res.*, *117*, B04107, doi:10.1029/2011JB009110.

Gailler, A., F. Klingelhoefer, J. L. Olivet, D. Aslanian, P. Sardinia Sci, and O. B. S. T. Tech (2009), Crustal structure of a young margin pair: New results across the Liguro-Provencal basin from wide-angle seismic tomography, *Earth Planet. Sci. Lett.*, *286*(1-2), 333–345, doi:10.1016/j.epsl.2009.07.001.

Gallastegui, J., J. A. Pulgar, and J. Gallart (2002), Initiation of an active margin at the North Iberian continent-ocean transition, *Tectonics*, *21*(4), 15-1–15-14, doi:10.1029/2001TC901046.

Gautier, F., G. Clauzon, J. P. Suc, J. Cravatte, and D. Violanti (1994), Age and duration of the Messinian salinity crisis, *C. R. Acad. Sci., Ser. II*, *318*(8), 1103–1109.

Gelabert, B., F. Sabat, and A. Rodriguez-Perea (2002), A new proposal for the late Cenozoic geodynamic evolution of the Western Mediterranean, *Terra Nova*, *14*(2), 93–100.

Geoffroy, L. (2005), Volcanic passive margins, *C. R. Geosci.*, *337*(16), 1395–1408.

Govers, R., and M. J. R. Wortel (2005), Lithosphere tearing at step faults: Response to edges of subduction zones, *Earth Planet. Sci. Lett.*, *236*(1-2), 505–523, doi:10.1016/j.epsl.2005.03.022.

Greenroyd, C. J., C. Peirce, M. Rodger, A. B. Watts, and R. W. Hobbs (2008), Demerara plateau—The structure and evolution of a transform passive margin, *Geophys. J. Int.*, *172*(2), 549–564, doi:10.1111/j.1365-246X.2007.03662.x.

Grevemeyer, I., C. Ranero, W. Leuchters, D. Pesquer, G. Booth-Rea, and J. Gallart (2011), Seismic constraints on the nature of crust in the Algerian-Balearic basin implications for lithospheric construction at back-arc spreading centers, *Eos Trans. AGU, Abstract T53D-04*.

Gueguen, E., C. Doglioni, and M. Fernandez (1998), On the post-25 Ma geodynamic evolution of the Western Mediterranean, *Tectonophysics*, *298*(1-3), 259–269.

Hirata, N., B. Y. Karp, T. Yamaguchi, T. Kanazawa, K. Suyehiro, J. Kasahara, H. Shiobara, M. Shinohara, and H. Kinoshita (1992), Oceanic-crust in the Japan basin of the Japan sea by the 1990 Japan-USSR Expedition, *Geophys. Res. Lett.*, *19*(20), 2027–2030.

Hinz, K. (1973), Crustal structure of Balearic Sea, *Tectonophysics*, *20*(1-4), 295–302.

Holbrook, W. S., et al. (2001), Mantle thermal structure and active upwelling during continental breakup in the North Atlantic, *Earth Planet. Sci. Lett.*, *190*(3-4), 251–266.

Horen, H., M. Zamora, and G. Dubuisson (1996), Seismic waves velocities and anisotropy in serpentinized peridotites from xigaze ophiolite: Abundance of serpentine in slow spreading ridge, *Geophys. Res. Lett.*, *23*(1), 9–12.

Hsu, K. J., M. B. Cita, and W. B. F. Ryan (1973), The origin of the Mediterranean evaporites, *Init. Rept. Deep Sea Drill. Proj.*, *13*, 1203–1231.

Johnson, H., et al. (eds.) (2008), *The Nature and Origin of Compression in Passive Margins*, vol. 306, Geol. Soc. London Sp. Pub., London.

Jolivet, L., and C. Faccenna (2000), Mediterranean extension and the Africa-Eurasia collision, *Tectonics*, *19*(6), 1095–1106, doi:10.1029/2000TC900018.

Keen, C. E., W. A. Kay, and W. R. Roest (1990), Crustal anatomy of a transform continental margin, *Tectonophysics*, *173*(1-4), 527–529.

Klingelhoefer, F., R. A. Edwards, R. W. Hobbs, and R. W. England (2005), Crustal structure of the NE Rockall Trough from wide-angle seismic data modeling, *J. Geophys. Res.*, *110*, B11105, doi:10.1029/2005JB003763.

Klingelhoefer, F., J. L. Olivet, D. Aslanian, F. Bache, M. Moulin, L. Matias, A. Afilhado, H. Nouze, M. O. Bellier, and A. Gailler (2008), Preliminary results from the Sardinia deep seismic cruise on the Western Sardinia and Gulf of Lions conjugate margin pair, *EGU meeting april 2008*, Vienna.

Klingelhoefer, F., C. Labails, E. Cosquer, S. Rouzo, L. Geli, D. Aslanian, J. L. Olivet, M. Sahabi, H. Nouze, and P. Unternehr (2009), Crustal structure of the SW-Moroccan margin from wide-angle and reflection seismic data (the DAKHLA experiment) part A: Wide-angle seismic models, *Tectonophysics*, *468*(1-4), 63–82, doi:10.1016/j.tecto.2008.07.022.

Korenaga, J., P. B. Kelemen, and W. S. Holbrook (2002), Methods for resolving the origin of large igneous provinces from crustal seismology, *J. Geophys. Res.*, *107*(B9), 2178, doi:10.1029/2001JB001030.

Krijgsman, W., F. J. Hilgen, I. Raffi, F. J. Sierro, and D. S. Wilson (1999), Chronology, causes and progression of the Messinian Salinity Crisis, *Nature*, *400*(6745), 652–655.

Lofi, J., F. Sage, J. Déverchère, L. Loncke, A. Maillard, V. Gaullier, I. Thinon, H. Gillet, P. Guennoc, and C. Gorini (2011), Refining our knowledge of the Messinian Salinity Crisis records in the offshore domain through multi-site seismic analysis, *Bull. Soc. Geol. Fr.*, *182*(2), 163–180.

Lonergan, L., and N. White (1997), Origin of the Betic-Rif mountain belt, *Tectonics*, *16*(3), 504–522, doi:10.1029/96TC03937.

Louden, K. E. (1980), The crustal and lithospheric thicknesses of the Philippine Sea as compared to the Pacific, *Earth Planet. Sci. Lett.*, *50*(1), 275–288.

Louden, K. E., and D. Chian (1999), The deep structure of non-volcanic rifted continental margins, *Philos. Trans. R. Soc. A Math. Phys. Eng. Sci.*, *357*(1753), 767–800.

Ludwig, J. W., J. E. Nafe, and C. L. Drake (1970), Seismic refraction, *Sea*, *4*(2), 55–84.

Maillard, A., and A. Mauffret (2013), Structure and present-day compression in the offshore area between Alicante and Ibiza island (Eastern Iberian margin), *Tectonophysics*, *591*, 116–130, doi:10.1016/j.tecto.2011.07.007.

Malinverno, A., and W. B. F. Ryan (1986), Extension in the Tyrrhenian Sea and shortening in the Apennines as result of arc migration driven by sinking of the lithosphere, *Tectonics*, *5*(2), 227–245, doi:10.1029/TC005i002p00227.

Martinez, F., F. M. K. Okino, Y. Ohara, A. L. Reysenbach, and S. K. Goffredi (2007), Back-arc basins, *Oceanography*, *20*(1), 116–127.

Mascle, J., and C. Basile (1998), Continental transform margins, *C. R. Acad. Sci., Ser. II A*, *326*(12), 827–838.

Mauffret, A., D. F. de Lamotte, S. Lallemant, C. Gorini, and A. Maillard (2004), E-W opening of the Algerian basin (Western Mediterranean), *Terra Nova*, *16*(5), 257–264.

Mauffret, A., A. Ammar, C. Gorini, and H. Jabour (2007), The Alboran Sea (Western Mediterranean) revisited with a view from the Moroccan margin, *Terra Nova*, *19*(3), 195–203.

Maury, R. C., et al. (2000), Post-collisional Neogene magmatism of the Mediterranean Maghreb margin: A consequence of slab breakoff, *C. R. Acad. Sci., Ser. II A*, *331*(3), 159–173.

Meghraoui, M., J. L. Morel, J. Andrieux, and M. Dahmani (1996), Pliocene and Quaternary tectonics of the Tell-Rif mountains and Alboran Sea, a complex zone of continent-continent convergence, *Bull. Soc. Geol. Fr.*, *167*(1), 141–157.

Montadert, L., J. Sancho, J. P. Fail, J. Debyser, and E. Winnock (1970), Tertiary age of saliferous series responsible for diapiric structures in Western Mediterranean (northeast of Baleares), *C. R. Hebd. Seances Acad. Sci. Ser. D*, *271*(10), 812–815.

Nocquet, J. M., and E. Calais (2004), Geodetic measurements of crustal deformation in the Western Mediterranean and Europe, *Pure Appl. Geophys.*, *161*(3), 661–681.

Pascal, G. P., A. Mauffret, and P. Patriat (1993), The ocean continent boundary in the Gulf of Lion from analysis of expanding spread profiles and gravity modeling, *Geophys. J. Int.*, *113*(3), 701–726.

Pepe, F., A. Sulli, G. Bertotti, and F. Cella (2010), Architecture and Neogene to recent evolution of the Western Calabrian continental margin: An upper plate perspective to the Ionian subduction system, Central Mediterranean, *Tectonics*, *29*, TC3007, doi:10.1029/2009TC002599.

Reid, I. D., and C. E. Keen (1990), High seismic velocities associated with reflections from within the lower oceanic-crust near the continental-margin of Eastern Canada, *Earth Planet. Sci. Lett.*, *99*(1-2), 118–126.

Ritchie, J. D., H. Johnson, M. F. Quinn, and R. W. Gatliff (2008), The effects of Cenozoic compression within the Faroe-Shetland Basin and adjacent areas, in *Nature and Origin of Compression in Passive Margins,* vol. 306, edited by H. Johnson et al., Geo. Soc, London, Sp. Pub, pp. 121–136.

Rollet, N., J. Déverchère, M. O. Beslier, P. Guennoc, J. P. Rehault, M. Sosson, and C. Truffert (2002), Back arc extension, tectonic inheritance, and volcanism in the Ligurian Sea, Western Mediterranean, *Tectonics*, *21*(3), 6-1–6-23, doi:10.1029/2001TC900027.

Rosenbaum, G., G. S. Lister, and C. Duboz (2002), Reconstruction of the tectonic evolution of the Western Mediterranean since the Oligocene, in *2002—Reconstruction of the evolution of the Alpine-Himalayan Orogen—Journal of the Virtual Explorer, 8*, edited by Rosenbaum, G., and G. S. Lister, 107–126, Virtual Explorer, Clear Range, NSW, Australia.

Roure, F., P. Casero, and B. Addoum (2012), Alpine inversion of the North African margin and delamination of its continental lithosphere, *Tectonics*, *31*, TC3006, doi:10.1029/2011TC002989.

Ryan, W. B. F., and M. B. Cita (1978), Nature and distribution of Messinian erosional surfaces—Indicators of a several-kilometer-deep Mediterranean in Miocene, *Mar. Geol.*, *27*(3-4), 193–230.

Sage, F., C. Basile, J. Mascle, B. Pontoise, and R. B. Whitmarsh (2000), Crustal structure of the continent-ocean transition off the Côte d'Ivoire-Ghana transform margin: Implications for thermal exchanges across the palaeotransform boundary, *Geophys. J. Int.*, *143*(3), 662–678.

Sage, F., G. Von Gronefeld, J. Déverchère, V. Gaullier, A. Maillard, and C. Gorini (2005), Seismic evidence for Messinian detrital deposits at the Western Sardinia margin, north Western Mediterranean, *Mar. Pet. Geol.*, *22*(6-7), 757–773.

Savoye, B., and D. J. W. Piper (1991), The Messinian event on the margin of the Mediterranean-sea in the Nice area, southern France, *Mar. Geol.*, *97*(3-4), 279–304.

Schettino, A., and E. Turco (2006), Plate kinematics of the western Mediterranean region during the Oligocene and early Miocene, *Geophys. J. Int.*, *166*(3), 1398–1423.

Serpelloni, E., G. Vannucci, S. Pondrelli, A. Argnani, G. Casula, M. Anzidei, P. Baldi, and P. Gasperini (2007), Kinematics of the Western Africa-Eurasia plate boundary from focal mechanisms and GPS data, *Geophys. J. Int.*, *169*(3), 1180–1200.

Sibuet, J. C. (1974), Histoire tectonique du Golfe de Gascogne, *Contribution du département Scientifique, Centre Océanologique de Bretagne*, *137*(155), 297–312.

Speranza, F., I. M. Villa, L. Sagnotti, F. Florindo, D. Cosentino, P. Cipollari, and M. Mattei (2002), Age of the Corsica-Sardinia rotation and Liguro-Provençal basin spreading: New paleornagnetic and Ar/Ar evidence, *Tectonophysics*, *347*(4), 231–251.

Stich, D., E. Serpelloni, F. D. Mancilla, and J. Morales (2006), Kinematics of the Iberia-Maghreb plate contact from seismic moment tensors and GPS observations, *Tectonophysics*, *426*(3-4), 295–317.

Stockwell, J. W. (1999), The CWP/SU: Seismic unix package, *Comput. Geosci.*, *25*(4), 415–419.

Strzerzynski, P., J. Déverchère, A. Cattaneo, A. Domzig, K. Yelles, B. M. de Lepinay, N. Babonneau, and A. Boudiaf (2010), Tectonic inheritance and Pliocene-Pleistocene inversion of the Algerian margin around Algiers: Insights from multibeam and seismic reflection data, *Tectonics*, *29*, TC2008, doi:10.1029/2009TC002547.

Thiébot, E. (2005), Structure profonde et réactivation de la marge nord-ouest Marocaine, Thèse de doctorat, UMR6538, IUEM, Université de Bretagne Occidentale.

Turner, I. M., C. Peirce, and M. C. Sinha (1999), Seismic imaging of the axial region of the Valu Fa Ridge, Lau basin—The accretionary processes of an intermediate back-arc spreading ridge, *Geophys. J. Int.*, *138*(2), 495–519.

Vidal, N., J. Gallart, and J. J. Danobeitia (1998), A deep seismic crustal transect from the NE Iberian peninsula to the Western Mediterranean, *J. Geophys. Res. Solid Earth*, *103*(B6), 12,381–12,396.

Wessel, P., and W. Smith (1995), New version of the generic mapping tool released, *Eos Trans. AGU*, *76*(33), 329, doi:10.1029/95EO00198.

White, R. S., D. McKenzie, and R. K. Onions (1992), Oceanic crustal thickness from seismic measurements and rare-earth element inversions, *J. Geophys. Res.*, *97*(B13), 19,683–19,715, doi:10.1029/92JB01749.

Whitmarsh, R. B., G. Manatschal, and T. A. Minshull (2001), Evolution of magma-poor continental margins from rifting to seafloor spreading, *Nature*, *413*(6852), 150–154.

Yelles, A., et al. (2009), Plio-quaternary reactivation of the Neogene margin off NW Algiers, Algeria: The Khayr al Din Bank, *Tectonophysics*, *475*(1), 98–116.

Zelt, C. A. (1999), Modelling strategies and model assessment for wide-angle seismic traveltime data, *Geophys. J. Int.*, *139*(1), 183–204.

Zelt, C. A., and R. B. Smith (1992), Seismic traveltime inversion for 2-D crustal velocity structure, *Geophys. J. Int.*, *108*(1), 16–34.

Ziegler, P. A., and S. Cloetingh (2004), Dynamic processes controlling evolution of rifted basins, *Earth Sci. Rev.*, *64*(1-2), 1–50, doi:10.1016/S0012-8252(03)00041-2.